

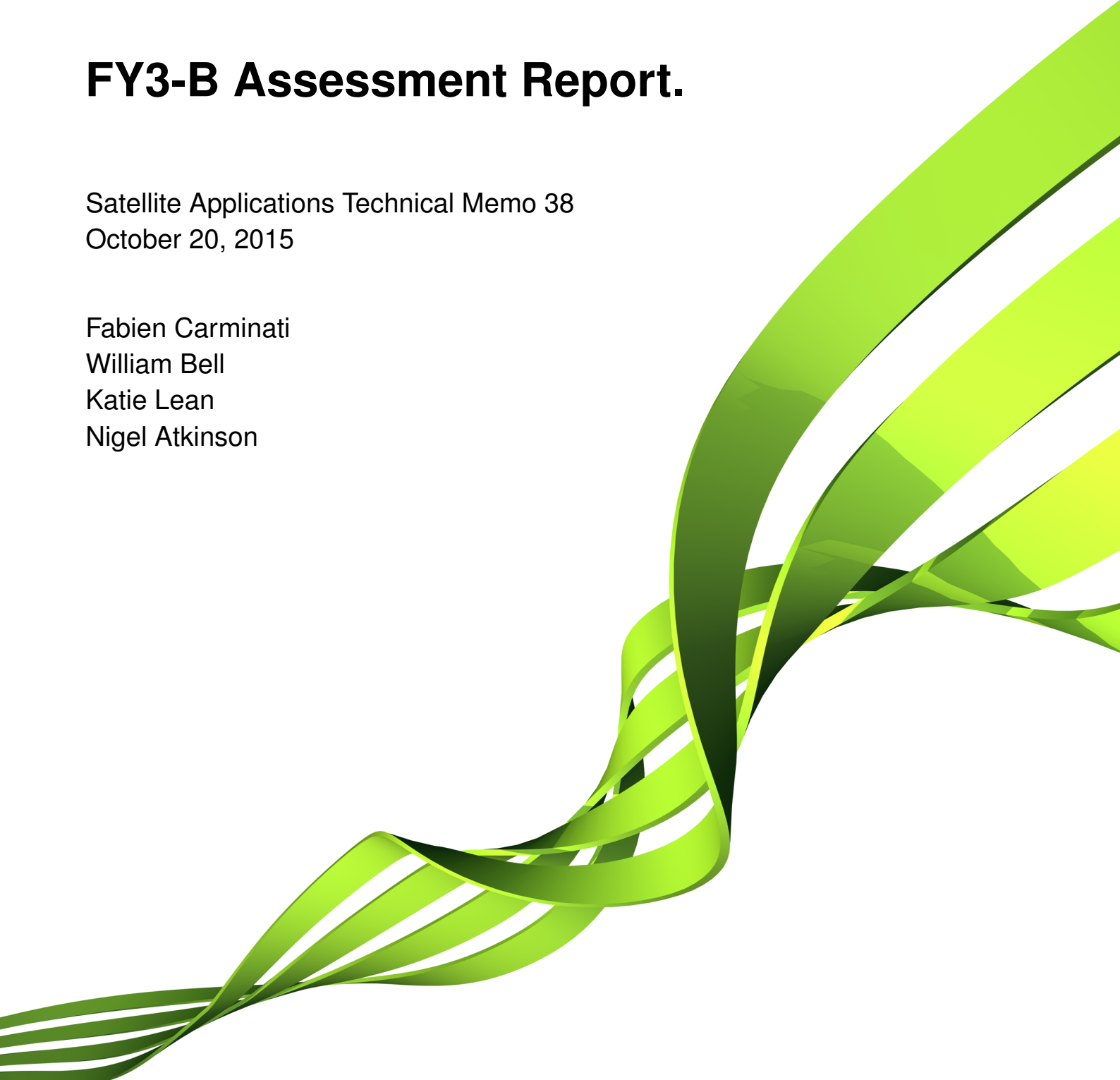


Met Office

FY3-B Assessment Report.

Satellite Applications Technical Memo 38
October 20, 2015

Fabien Carminati
William Bell
Katie Lean
Nigel Atkinson



Contents

Abstract	2
1 Introduction	3
2 Data quality assessment	6
2.1 Data characteristics in 2013	6
2.1.1 First guess departure	7
2.1.2 Scan position dependency	13
2.1.3 Radiometer non-linearity	15
2.2 Data characteristics in 2015	17
3 Assimilation Experiment	20
3.1 VAR statistics	20
3.2 NWP index	22
Conclusion	25
Appendix A	27
Appendix B	29
Appendix C	32
Appendix D	33
Appendix E	34
References	38

Abstract

China's Feng-Yun 3 (FY-3) platforms are a series of polar orbiting satellites which will become a major source of data for numerical weather prediction (NWP) and climate monitoring over the next two decades. The Microwave Humidity Sounder 1 (MWHS-1) and the Microwave Temperature Sounder 1 (MWTS-1) were launched as experimental instruments on board FY-3B in 2010. Observations from both instruments have been assessed for their assimilation in the Met Office NWP model. The comparison of one year of observations with NWP background fields revealed biases affected by seasonal modulation, surface type, scan position, and scene temperature. Except for window sensitive channels, the Met Office static bias correction scheme, and to a greater extent the new variational bias correction scheme, result to be effective in reducing most of the observed biases to operational quality standards. An assimilation experiment in NWP results in a mostly neutral impact, both on NWP indexes and in the fit of observations to model short range forecasts for independent humidity sensors.

1 Introduction

The National Satellite Meteorological Center (NSMC) of Chinese Meteorological Administration (CMA) has been developing since the 80's a space-borne-based network of Earth observing systems involving both polar-orbiting and geostationary satellites. The 20-year long phase 3 of the Feng-Yun (Wind and Cloud in Chinese) program (FY-3) began in 2008 with the launch of the first new generation polar-orbiting platform FY-3A (Dong et al., 2009), followed by FY-3B in 2010 and FY-3C in 2013. Four other platform (FY-3D, E, F and G) will complete the fleet between 2016 and 2022. Launches take place on 2-year intervals, placing the platforms alternately on a morning and an afternoon orbit.

The principal objectives of the FY-3 program are: i) the support of numerical weather prediction (NWP) with temperature, moisture, cloud, and precipitation observations, ii) make available geophysical parameters for climate monitoring support, and iii) provide biosphere, hydrological and meteorological imagery. CMA is also aiming at collecting and relaying data at ground segments as well as ensuring an operational phase with a minimum of two working satellites (<http://www.nsmc.cma.gov.cn/en/NSMC/Home/index.html>).

Both FY-3A and B were designed as experimental platforms with an expected life-time of 2 years. Hence, their sounding capability is limited with respect to the following platforms designed for operational use and 5 years life-time.

FY-3B, launched on November 04, 2010, has an orbit crossing the equator on ascending node at 13:40 local time. The platform carries eleven instruments:

- the Earth Radiation Measurement 1 (ERM-1),
- the Infra Red Atmospheric Sounder (IRAS),
- the MEdium Resolution Spectral Imager 1 (MERSI-1),
- the MicroWave Humidity Sounder 1 (MWHS-1),
- the MicroWave Radiation Imager (MWRI),
- the MicroWave Temperature Sounder 1 (MWTS-1),
- the Solar Backscatter Ultraviolet Sounder (SBUS),
- the Space Environment Monitor (SEM),
- the Solar Irradiance Monitor 1 (SIM-1),
- the Total Ozone Unit (TOU) and,
- the Visible and Infra Red Radiometer (VIRR)

This document focuses on MWTS-1 and MWHS-1.

MWTS-1 is a 4-channel sounder covering the 50-57 GHz spectral range. The scanning geometry results in an along-track line of 118 km every 16 s, and a cross-track scan of 15 steps of 62 km at nadir. The total swath is 2088 km (or $\pm 48.6^\circ$). MWHS-1 has 5 channels covering the 150-183 GHz spectral range. The scanning geometry allows 15 km lines every 2.6 s along-track, while the cross-track scan is made up of 98 steps of 16 km at nadir for a total swath of 2692 km ($\pm 53.38^\circ$). MWTS-1 and MWHS-1 characteristics are further details in Table 1 and 2, respectively.

Table 1: MWTS-1 channel characteristics and equivalent channels for MWTS-2, ATMS and AMSU-A.

MWTS-1						Equivalent channels		
Channel Number	Central Frequency (GHz)	Polarization	Bandwidth (MHz)	Main Absorber	NEΔT (K)	FY-3C (MWTS-2)	ATMS	AMSU A
1	50.3	H	180	window	0.5	1	3	3
2	53.6	H	340	O ₂	0.4	4	6	5
3	54.94	H	400	O ₂	0.4	6	8	7
4	57.29	H	330	O ₂	0.4	8	10	9

Table 2: MWHS-1 channel characteristics and equivalent channels for MHTS-2, ATMS and AMSU-B/MHS.

MWHS-1						Equivalent channels		
Channel Number	Central Frequency (GHz)	Polarization	Bandwidth (MHz)	Main Absorber	NEΔT (K)	FY-3C (MWHS-2)	ATMS	AMSU B - MHS
1	150	V	1001	window	0.9	10	-	2
2	150	H	987	window	0.71	-	-	-
3	183.31±1	V	481	H ₂ O	1.01	11	22	3
4	183.31±3	V	1034	H ₂ O	1.06	13	20	4
5	183.31±7	V	2186	H ₂ O	1.19	15	18	5

Assessments were conducted for both MWTS-1 and MWHS-1 (Zou et al., 2011; Lu et al., 2011a, 2011b, 2012; Chen et al., 2014), but mostly focused on the instruments on board FY-3A. Lu et al. (2011a and b), which focused on MWTS-1, identified two distinct biases using ECMWF NWP and radiative transfer models, as well as comparisons with equivalent observations from the Advanced Microwave Sounding Unit-A (AMSU-A), a long-time used instrument for assimilation in NWP. Shifts in frequency of 55, 39, and 33 MHz in channel passbands were observed in channels 2, 3, and 4, respectively. Also, a radiometer nonlinearity linked to temperature dependence scene was shown to cause a positive bias in observation of brightness temperature. Similar conclusions were

drawn by Zou et al. (2011). Overall, all studies agree that, after appropriate correction, MWTS-1 compares well to AMSU-A equivalent channels and improve forecast accuracy when assimilated in NWP models.

In an ECMWF technical report, Chen et al. (2014) carried out a comprehensive analysis of FY-3A and B MWHS-1 observations. Compared to equivalent channels of similar instruments, they showed the MWHS-1 ratio of noise equivalent delta temperature ($NE\Delta T$) to be larger than that of the Microwave Humidity Sounder (MHS) on the European platform MetOp-B, but smaller than AMSU-B $NE\Delta T$ on US platforms NOAA-15, 16 and 17. The first guess departure was also observed to be larger than in MHS observations and found to vary with the scan position. This scan dependent bias, also observed by Lu et al. (2011b), is larger for the instrument on FY-3A than on FY-3B. Assimilation experiments into the ECMWF Integrated Forecasting System (IFS) resulted in a neutral to slightly positive impact, with benefits observed in the fit of observations to the model for independent sensors in short-range forecasts, slight improvement in long-range forecasts, and reduction of forecast error in extra-tropics. Minor negative impact was found in the Tropics.

The present document deals in first instance with the analysis of biases in the FY-3B MWTS-1 and MWHS-1 observations over a 12-month time periods in 2013 and over a 5-day time period in 2015, presented in section 2. Results from an assimilation experiment are presented in section 3. Concluding remarks and recommendations finalize the document.

2 Data quality assessment

FY-3B MWTS-1 and MWHS-1 data have been received at the Met Office (MO) via the EUMETCast dissemination system since May 2012. Automatic archiving into the MO database was in place until the failure of MWTS-1 on February 2014. Archiving of MWHS-1 alone has restarted since April 2015 for the purpose of the assimilation experiment presented in this document and it is possible operational use. The data timeliness of 7.04 ± 2.65 h, estimated from the three first days after archiving restoration, is at the edge of the window for operational use (6.7 h), so that only about $36 \pm 29\%$ of the data are processed.

2.1 Data characteristics in 2013

In the 2013 version, MWHS-1 98 fields of view are mapped into MWTS-1 15 cross-track scan positions (in order to avoid oversampling) ahead of their introduction in the processing system. In the Observation Processing System (OPS), observation quality controls, bias correction, and retrieval of physical parameters are carried out in a similar way for all the instruments. Specific quality controls, channel selection, or thinning control can also be applied case by case.

For FY-3B humidity sounder, the *mwbcloudy* cirrus cloud cost test has been implemented and acts as a cost function imposing a threshold on the magnitude of the first guess departure at 183 ± 7 GHz (MWHS-1 channel 5), which can reject observations from MWHS-1 channels 4 and 5. Due to modeling issues, window channels sensitive to surface emissivity (MWTS-1 channel 1, and MWHS-1 channels 1 and 2) have been deactivated such as they can be used for quality control but not in the system processing. MWTS-1 channel 1 and 2 are rejected over land, while MWTS-1 channel 1 and MWHS-1 channel 3, 4, and 5 are rejected over sea ice. MWTS-1 channel 4 (57.29 GHz) has been producing spurious observations and was consequently deactivated both for quality control and processing. A summary of channel selection is available in Table 3.

Table 3: MWTS-1 and MWHS-1 channel rejections as a function of the surface type and clouds.

Flag	Rejection	
	MWTS-1	MWHS-1
Land	1, 2	-
Sea Ice	1	3, 4, 5
<i>mwbcloudy</i>	-	4, 5

Thinning controls for FY-3B temperature and humidity sounders are similar to those used for similar instruments such as Advanced Television and infrared observational satellite Operational Vertical Sounder (ATOVS), i.e. a 25 km thinning in 1-hour window followed by a 80 km thinning in 1-hour window.

MWTS-1 observation errors in OPS are derived from the Advanced Technology Microwave Sounder (ATMS) errors at equivalent channels scaled by the ratio of $NE\Delta T$, in similar way as described by Doherty et al. (2012). The same methodology is used to derive errors in the VARiational data assimilation system (VAR). MWHS-1 window channels (1 and 2) have been given the same errors as for MHS equivalent channels on MetOp-B, both in OPS and VAR. MWHS-1 channels 3 to 5 have been given the same errors as for ATMS equivalent channels, both in OPS and VAR. Unlike for MWTS-1, MWHS-1 errors are not scaled down by the ratio of $NE\Delta T$. Hence, the impact of a reduction of MWHS-1 errors will require further investigations. Table 4 summarizes MWTS-1 and MWHS-1 errors.

Table 4: MWTS-1 and MWHS-1 observation and forward model errors used in OPS and VAR.

	Channel #	MWTS-1				MWHS-1				
		1	2	3	4	1	2	3	4	5
Error (K)	OPS	1.220	0.144	0.146	0.183	5.000	5.000	4.500	4.000	4.000
	VAR	1.116	0.154	0.146	0.183	5.000	5.000	4.500	4.000	4.000

The MO static bias correction scheme (Harris and Kelly, 2001) has been implemented for MWTS-1 and MWHS-1 observations processing in OPS. Initially set to zero, a constant offset, two predictor values (representative of the atmospheric thickness at 850 and 200 hPa), and a set of coefficients for each scan position were calculated for each channel from 5 days of statistics (1-5 December 2013). This first round of coefficients was next used to generate a whole month of statistics (December 2013) and to recalculated a more accurate version of the coefficients. Finally, the second round of coefficients was used to generate another month of statistics (August 2013) from which was calculated the final version of the coefficients for the bias correction.

2.1.1 First guess departure

In this section, the first guess departure from raw observations (O-B) and the first guess departure from bias-corrected observations (C-B) are analyzed from January to December 2013. Both O-B and C-B are calculated after quality controls screening described in the channels selection. Results are presented as a function of the latitude and of the surface type. Table 5 summarizes the number of available observations each month (all channels and all latitudes included) as a function of the surface type, before and after screening.

Table 5: Total number of observations in million ($\times 10^6$) from January to December 2013, as a function of the surface type. The left columns show the number of raw data. The right columns show the number of data after quality control screening.

	Surface type	Raw				QC			
		Land	Ocean	Sea ice	Total	Land	Ocean	Sea ice	Total
Month	January	13.2	12.6	2.1	27.9	2.8	7.4	0.4	10.6
	February	11.7	11.2	1.8	24.7	2.5	6.7	0.3	9.5
	March	1.3	1.3	0.2	2.8	0.3	0.8	0.04	1.1
	April	2.5	2.3	0.4	5.2	0.6	1.4	0.1	2.1
	May	12.6	11.5	2.4	26.5	3.3	6.5	0.6	10.4
	June	12.1	11.1	2.3	25.5	3.5	6.4	0.7	10.6
	July	13.0	12.0	2.4	27.4	3.8	6.8	0.8	11.3
	August	10.6	9.9	1.9	22.4	3.0	5.6	0.5	9.1
	September	11.8	11.0	2.0	24.8	3.3	6.3	0.4	10.0
	October	12.7	11.6	2.4	26.7	3.5	7.0	0.4	10.9
	November	11.9	10.7	2.4	25.0	2.6	5.1	0.4	8.1
	December	12.6	11.6	2.5	26.7	2.2	4.1	0.4	6.7

MWTS-1

Figure 1 shows MWTS-1 channels 1 to 3 O-B (circles), C-B (filled circles), and their 1σ standard deviation (dashed and solid vertical bars, respectively), monthly averaged over oceanic surface in the northern and southern mid-latitudes ($20\text{--}60^\circ$).

A positive bias up to 1.5 K is observed for the O-B in Ch. 1. Conversely, the bias is mostly negative (down to -1.1 K) in Ch. 2 and 3. A marked seasonal effect is visible in Ch. 1 and 2, most likely because those are channels sensitive to surface and lower tropospheric emissions. A seasonal variability is also visible, although to a lesser extent, in Ch. 3, consistent with the peak of sensitivity in the upper troposphere where seasonal variation of temperature are less marked than at the surface. This also explains the smaller standard deviations observed in Ch. 3 compared to the two other channels. C-B is, in most cases, smaller than O-B, except in the boreal winter in Ch. 2, and atypical peaks only spotted in Ch. 3. The seasonal effect is also attenuated when considering the corrected data set. The largest impact appears to be for Ch. 1, where the amplitude of the seasonal variability is reduced by 0.5 K.

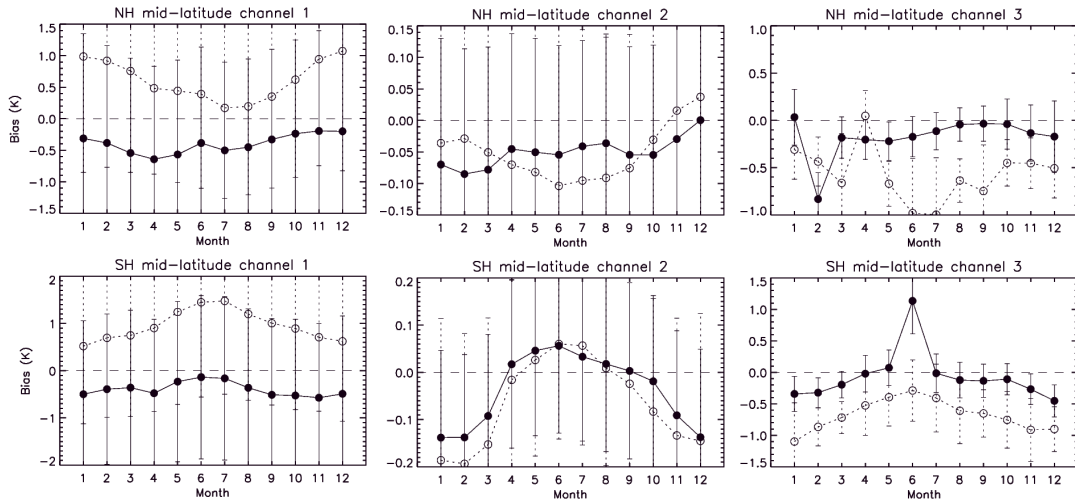


Figure 1: (Top, from left to right) Monthly averaged O-B (circles), C-B (filled circles), and 1σ standard deviation (dashed and solid vertical bars, respectively) for MWTS-1 channels 1 to 3 over mid-latitudes oceanic surface in the northern hemisphere. (Bottom) Same as top, but for the southern hemisphere.

Fig. 2 is similar to Fig. 1 but over land surface and Ch. 3 only. O-B is mostly negative (down to 0.9 K), and again presents atypical peaks in both hemispheres. No obvious seasonal variability is observed. The bias correction results in significant improvements as most of C-B is within 0.3 K to zero.

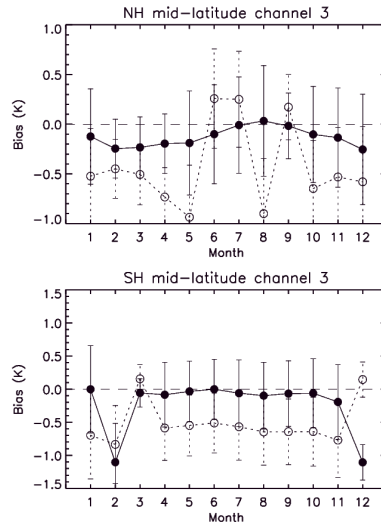


Figure 2: Same as Fig. 1, but for land surface, channel 3 only.

Figures showing MWTS-1 O-B and C-B over land, oceanic, and sea ice surfaces in polar regions ($60\text{--}90^\circ$) as well as in the tropics ($\pm 20^\circ$) are available in Appendix A. In polar regions, most of the patterns observed in Figs. 1 and 2 are similar. Noteworthy differences are: i) larger bias in O-B over

ocean although not necessarily larger C-B, and ii) the seasonal variability disappears from Ch. 1, but appears in Ch. 3. The former point remains unexplained. In the tropics, O-B and C-B are smaller than in extra-tropics (except in Ch. 2 oceanic surface). No seasonal variability is observed.

Table 6 summarizes for each channel and each surface type the O-B, C-B, and their 1σ standard deviations averaged over the whole year at all latitudes. MWTS-1 O-B varies from -0.58 to 1.42 K and C-B varies from -0.24 to -0.1 K. The standard deviation does not present significant improvements.

Table 6: MWTS-1 channels 1 to 4 (left) and MWHS-1 channels 1 to 5 (right) O-B, C-B, and 1σ standard deviation over oceanic (top), land (middle), and sea ice (bottom row) surfaces yearly-averaged (2013) at all latitudes.

K ($\pm 1\sigma$)		MWTS-1				MWHS-1				
		Ch 1	Ch 2	Ch 3	Ch 4	Ch 1	Ch 2	Ch 3	Ch 4	Ch 5
Ocean	O-B	1.42 (± 1.87)	-0.12 (± 0.17)	-0.58 (± 0.13)	-	0.01 (± 3.18)	-0.89 (± 2.42)	-2.21 (± 1.65)	-2.25 (± 1.10)	-0.86 (± 1.24)
	C-B	-0.10 (± 1.80)	-0.10 (± 0.14)	-0.10 (± 0.20)	-	1.27 (± 2.65)	0.83 (± 2.61)	-0.26 (± 1.58)	-0.36 (± 0.98)	-0.27 (± 0.95)
Land	O-B	-	-	-0.51 (± 0.21)	-	-6.52 (± 2.61)	-6.10 (± 2.05)	-2.04 (± 1.75)	-2.17 (± 1.35)	-1.41 (± 1.65)
	C-B	-	-	-0.16 (± 0.21)	-	-5.44 (± 2.61)	-4.52 (± 2.05)	-0.15 (± 1.75)	-0.30 (± 1.35)	-1.03 (± 1.65)
Sea ice	O-B	-	-0.27 (± 0.20)	-0.55 (± 0.27)	-	-13.39 (± 5.27)	-12.18 (± 0.64)	-	-	-
	C-B	-	-0.17 (± 0.22)	-0.24 (± 1.52)	-	-13.75 (± 6.84)	-10.81 (± 0.61)	-	-	-

MWHS-1

Note that in the MO system, MWTS-1 and MWHS-1 are processed as one instrument with 9 channels, and therefore MWHS-1 Chs. 1 to 5 are referred to as Chs. 5 to 9. Fig. 3 and 4 are similar to Fig. 1 but for MWHS-1 Chs. 5 and 6 (150 GHz window channels), and Chs. 7, 8, and 9 (183 GHz channels), respectively.

MWHS-1 window channels shown on Fig. 3 present negative O-B down to -0.5 K in Ch. 5 and -2.4 K in Ch. 6. The impact of the seasons is mostly visible in the southern hemisphere where the amplitude is about 1 K. In contrast, O-B in northern mid-latitudes has less variability and smaller biases. Except for Ch. 5 austral winter, the bias correction improves the first guess departure with C-B mostly within ± 0.5 K. Seasonal impact on C-B is also visible in the southern hemisphere, although with a slight reduction in amplitude with respect to O-B.

The 183 GHz channels shown on Fig. 4 all present a negative O-B. The departure ranges from -0.7 to -0.1 K in the near-surface peaking Ch. 9, and around -2 K for high peaking Ch. 7 and 8. The impact of the season, predominant in the northern hemisphere, remains however minor (<0.5 K

amplitude) relative to that of the window channels. Again, C-B is much smaller than O-B, and ranges within ± 0.5 K.

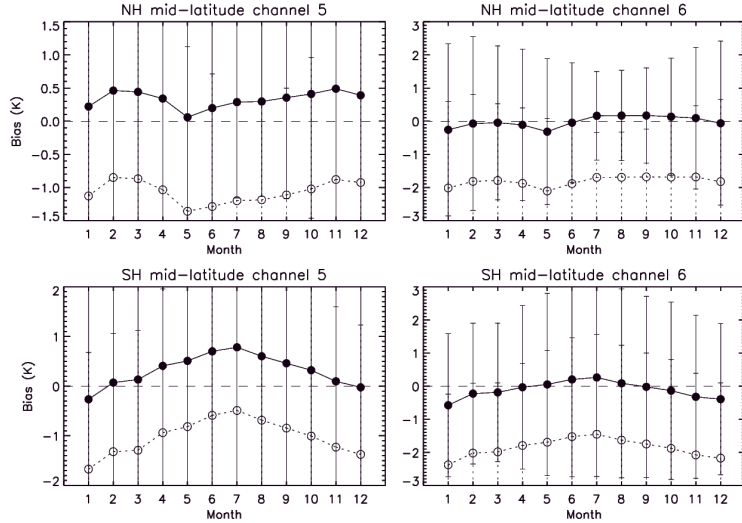


Figure 3: (Top, from left to right) Monthly averaged O-B (circles), C-B (filled circles), and 1σ standard deviation (dashed and solid vertical bars, respectively) for MWHS-1 channels 5 and 6 over mid-latitudes oceanic surface in the northern hemisphere. (Bottom) Same as top, but for the southern hemisphere.

Figs. 5 and 6 are similar to Figs. 3 and 4 but for land surface. Compared to oceanic surface, window channels over land (Fig. 5) have larger biases (down to -6 K) and more marked seasonal cycles (4 K amplitude) in the northern hemisphere, but smaller biases (down to -1 K) and seasonal cycles nearly absent (<0.5 K) in the southern hemisphere. The bias correction result in a small degradation of C-B with respect to O-B in the austral summer.

183 GHz channels over land (Fig. 6) have relatively similar characteristics to those over ocean. Significant differences are: i) a positive C-B in Ch. 7 southern mid-latitudes characterized by a larger seasonal cycle than over ocean, and ii) year-round mostly positive O-B and C-B in Ch. 9 southern mid-latitudes, also characterized by a significant seasonal variability. It is not surprising that window channels and Ch. 9 (peaking in the lowermost troposphere) are subject to larger seasonal variations above land where seasonal contrasts are stronger than above ocean. More of a concern is the Ch. 7 (mid-troposphere peak) 1 K seasonal amplitude, which might require further investigations. Another noteworthy feature is the Chs. 7 and 8 ~ 1 K difference between O-B over land and O-B over ocean in the Southern mid-latitudes. Channels 7 and 8 are mid-tropospheric peaking channels and therefore should not present a surface dependency. Other than an instrumental issue, a sampling effect caused by the small fraction of land with respect to ocean in this latitude band, and thus the lesser number of available observations, can, at least, partly explain such bias.

Figures showing polar and tropical regions over oceanic, land, and sea ice surfaces are available

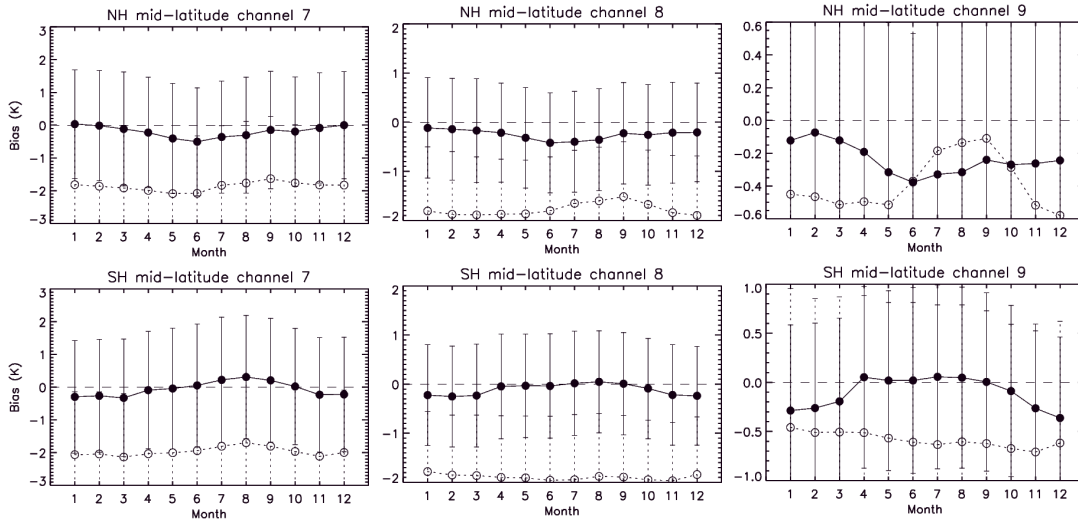


Figure 4: Same as Fig. 3 but for channels 7, 8, and 9.

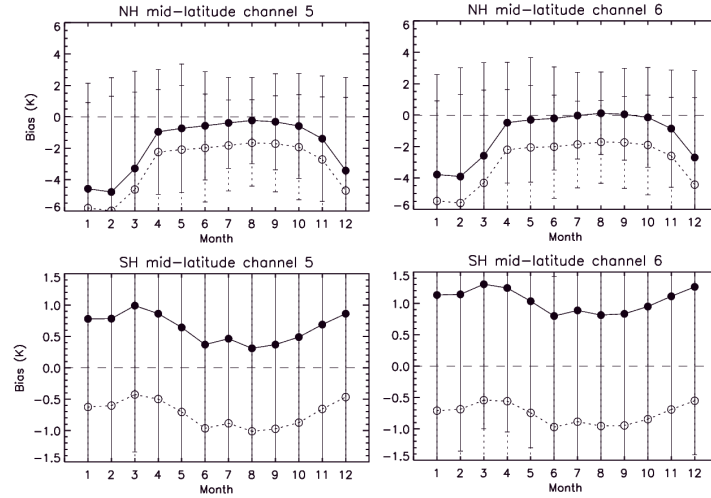


Figure 5: Same as Fig. 3 but for land surface.

in Appendix B. The most notable feature is a degradation of C-B with respect to O-B in the window channels over the southern polar oceanic region, as well as in the 183 GHz Ch. 9 over the tropical land region. Lastly, we can also note a positive O-B (0.2-0.4 K) seen in Ch. 9 in the tropics over ocean.

Table 6 summarizes MWHS-1 O-B, C-B, and their standard deviations. In summary, window channels biases are small over ocean ($O-B > -1$ K), but large over land (< -6 K) and even larger over ice (< -12 K). The correction scheme does not improve departures over ocean and ice for Ch. 5 (referred to as Ch. 1 in table 6). In contrast, the 183 GHz channels present relatively small O-B ranging from -0.86 to -2.25 K and systematic smaller C-B ranging from -0.15 to -1.03 K.

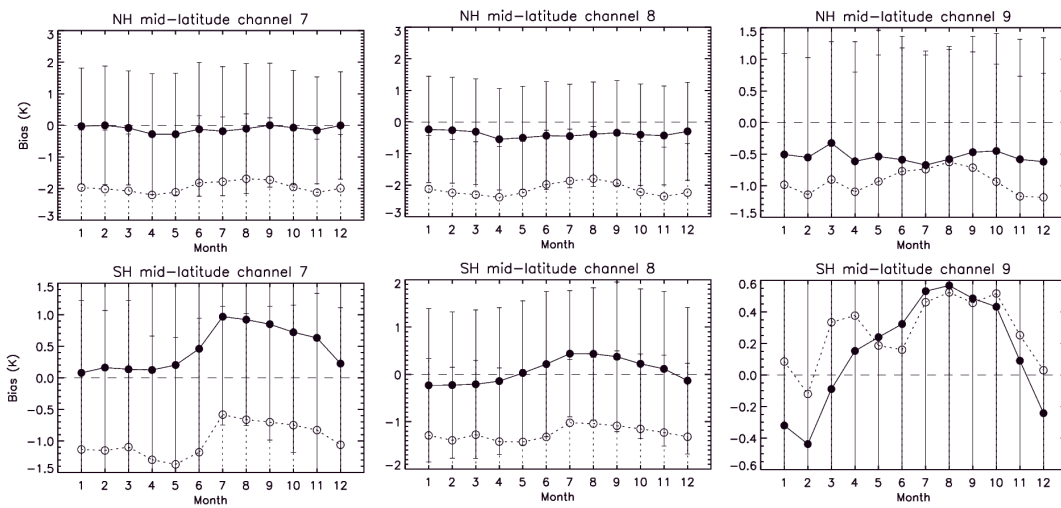


Figure 6: Same as Fig. 3 but for land surface channels 7, 8, and 9.

2.1.2 Scan position dependency

Early assessments of MWTS-1 and MWHS-1 (e.g. Chen et al., 2014) revealed variations of first guess departures as a function of the scan position. In this study, monthly-averaged O-B and C-B are analyzed as function of the scan position for both instruments, discriminating the surface type as well as the latitude band. Because the scan position dependency is not found to vary significantly over the year, the results presented in this report focus on July 2013.

Fig. 7 shows the variations in first guess departure in raw observations ($\Delta O-B$) with the scan positions in 14 latitude bands over oceanic surface. Note that for better readability, an offset setting to zero the middle scan position was applied to all $\Delta O-B$. Hence, this figure can only inform on the difference (in K) between two scan positions of a given latitude band, but neither the actual O-B nor the difference between two latitude bands. The black dashed line show the standard deviation of the 14 $\Delta O-B$ before offset.

Three main patterns emerge from the different channels:

- A dome shape pattern (Chs. 1 and 3) with 1-3 K amplitude between the edges and the middle of the scan. Largest amplitudes are found for high latitudes in Ch. 1 and the opposite in Ch. 3.
- A tilted shape pattern (Chs. 2, 7, and 8) with 0.5-2 K amplitude between the first and last scan position. This bias is more pronounced in MWHS-1 channels.
- A variable shape pattern (Chs. 5, 6, and 9), which shows local peaks and troughs with 1-5 K amplitude.

Although more irregular, those three patterns are also found over land and over sea ice (see Appendix C).

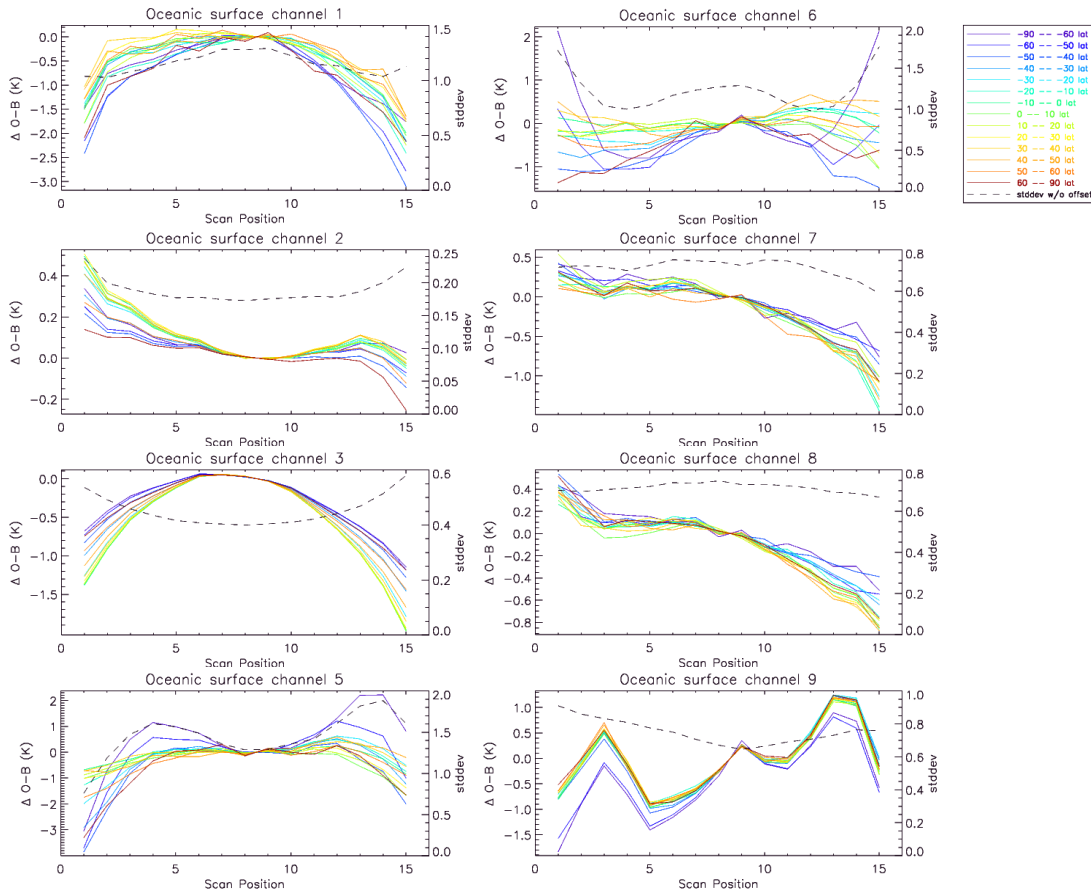


Figure 7: MWTS-1 channel 1, 2, and 3, and MWHS-1 channel 5, 6, 7, 8, and 9 variations in first guess departure in raw observations ($\Delta O-B$) as a function of scan position in 14 latitude bands over oceanic surface in July 2013. An offset was applied so that all $\Delta O-B$ are set to zero on the middle of the scan. Black dashed line shows the 1σ standard deviation of $\Delta O-B$ before offset.

Fig. 8 is similar to Fig. 7 but for bias-corrected data. Except for MWHS-1 window channels 5 and 6, the correction scheme significantly reduces the biases, decreases the standard deviation, and attenuates the patterns observed for $\Delta O-B$. Most of $\Delta C-B$ s lie within ± 0.5 K, with amplitudes reduced by as much as 60-90% compared to ΔO -Bs at equivalent channels and equivalent latitude bands. Standard deviation between ΔC -Bs is, on average, ~ 0.4 K ($\sim 60\%$) smaller than between ΔO -Bs (not considering Chs. 5 and 6). Similar improvements are also visible over land and over ice surfaces (see Appendix D).

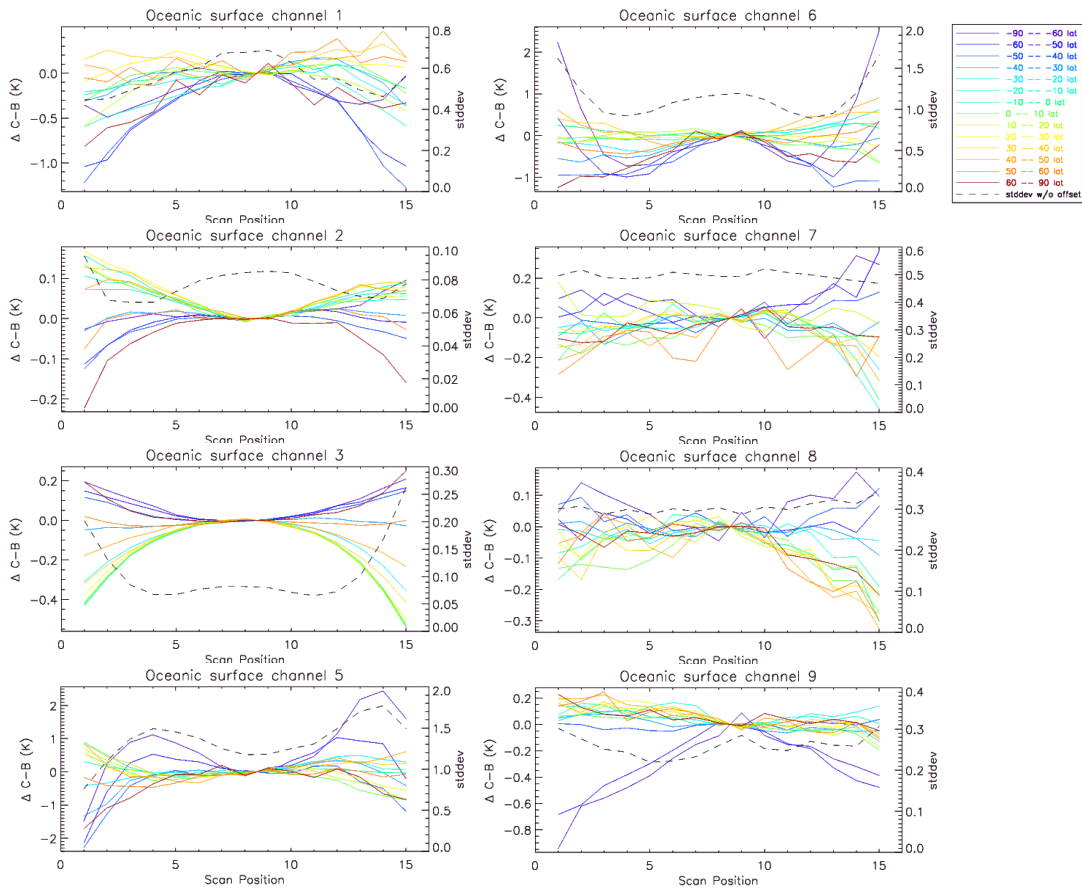


Figure 8: Same as Fig. 7 but for corrected data.

2.1.3 Radiometer non-linearity

A radiometer non-linearity, that is to say a deviation from the linear assumption in the interpolation between the instrument cold and warm calibration sources, was observed and documented for MWTS-1 (Lu et al., 2011a and b; Zou et al., 2011). This document focuses on the non-linearity assessment of MWHS-1. For this study, the dependence of O-B and C-B on scene temperature was analyzed from January to December 2013. Because it was found to vary little over the year, only the month of January is presented in this document.

The left column on Fig. 9 shows the biases as a function of the temperature for MWHS-1 Ch. 9 considering all raw observations (top), screened raw observations (middle), and screened-corrected observations (bottom). The right column shows the number of observations as a function of the temperature. Both raw and screened raw observation counts present a bimodal distribution with a minor peak around 260 K and a main peak around 280 K. Both bias distributions have a positive slope with negative O-B in the lower end of the temperature range, and positive O-B in its upper end. C-B distribution is characterized by a somehow flattened-slightly positive slope, meaning that the correction partly compensates for the radiometer non-linearity.

Chs. 5 to 8 are available in Appendix E. Ch. 8 has rather similar characteristics to Ch. 9 except for an observation count peaking around 250 K and to a lesser extent at 270 K. Ch. 7 presents a single peak of observation around 240 K and O-B distributions similar to those observed in Chs. 8 and 9. However, C-B distribution presents a steeper positive slope, synonymous of a lesser impact of the correction scheme on the radiometer non-linearity in the mid-troposphere. MWHS-1 window channels 5 and 6 have a peak of observation around 285 K preceded by a long tail reaching temperature below 220 K. O-B and C-B are relatively similar.

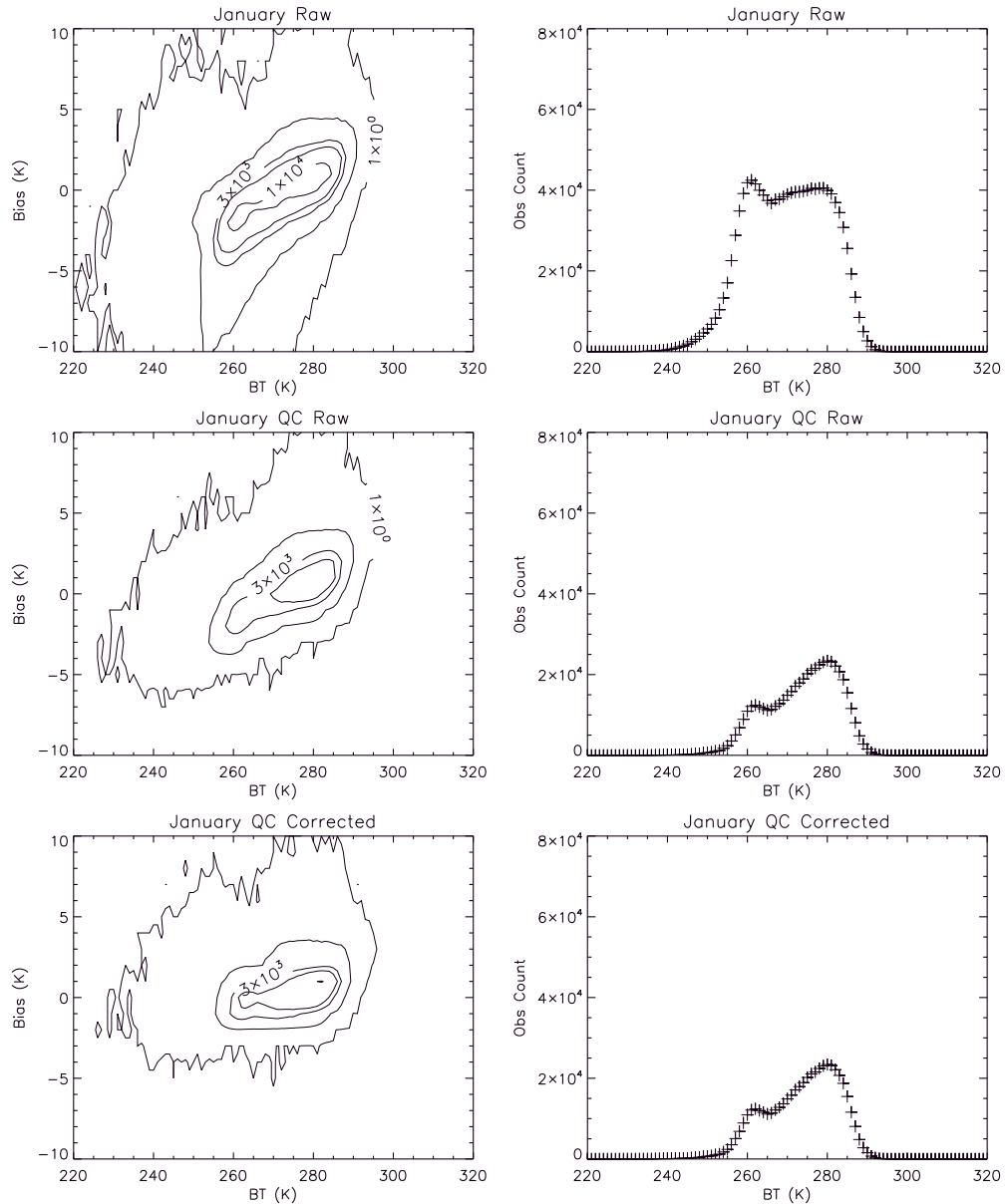


Figure 9: (Left) Distribution of MWHS-1 channel 9 O-B before quality control (top), quality control screened O-B (middle), and screened corrected (bottom) as a function of the brightness temperature (BT) in January 2013. (Right) Number of raw (top), screened raw (middle), and screened corrected observations (bottom).

2.2 Data characteristics in 2015

After the failure of MWTS-1 in February 2014, FY-3B data have not been archived in the MO system until recently. Observations from MWHS-1 alone are re-archived since April 22, 2015. Without temperature field to map humidity data, MWHS-1 observations are now archived with 49 samples per scan after averaging (instead of 15). Because 2015 data are aimed to be used in assimilation experiments, a few characteristics have been modified with respect to the 2013 version. First, all MWTS-1 channels are rejected both for quality controls and processing. Second, the assimilation experiments use a variational bias correction (VarBC) scheme (Cameron, 2015). In order to initiate VarBC, an input dataset, based on the static correction, have been generated. Following the same methodology as for 2013 data, the 5 first re-archived days (April 22-26) were used to generate static bias coefficients, and reprocessed with the static correction in order to compare the validity of data in 2015 with 2013. Because only MWHS-1 channels 7, 8, and 9 are aimed to be assimilated, the assessment focuses on those channels only.

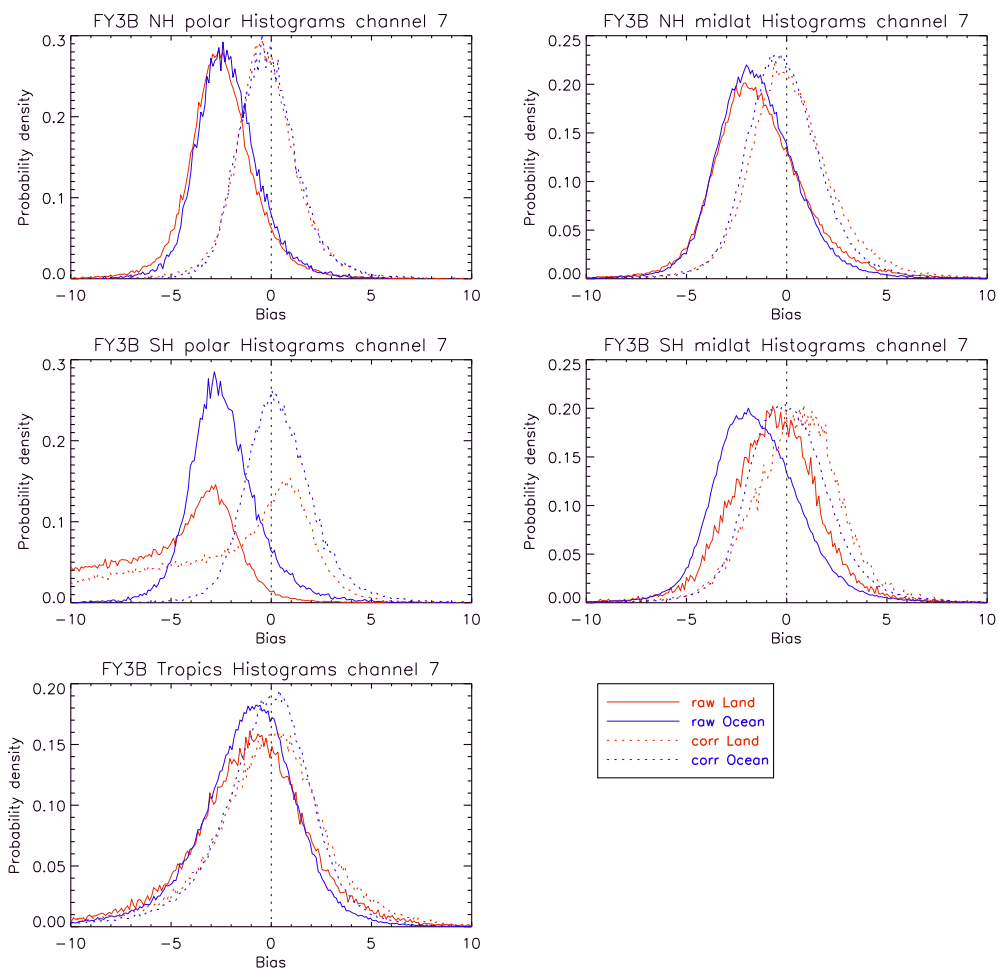


Figure 10: (From top to bottom and left to right) Histogram of O-B (solid lines) and C-B (dashed lines) expressed in Kelvin over northern and southern polar, mid-latitudes, and tropical land (red) and oceanic surfaces (blue) calculated for MWHS-1 channel 7 from April 22 to 26, 2015.

Figs. 10 to 12 show O-B (solid lines) and C-B (dashed lines) 5-day histograms for Chs. 7 to 9, respectively, over land (red) and oceanic surfaces (blue) in polar, mid-latitudes, and tropical areas. For all 3 channels, O-B range from -3 to 0 K, while C-B lies within ± 1 K (except Ch. 9 over land polar regions). Those biases are consistent with the biases found in the 2013 data.

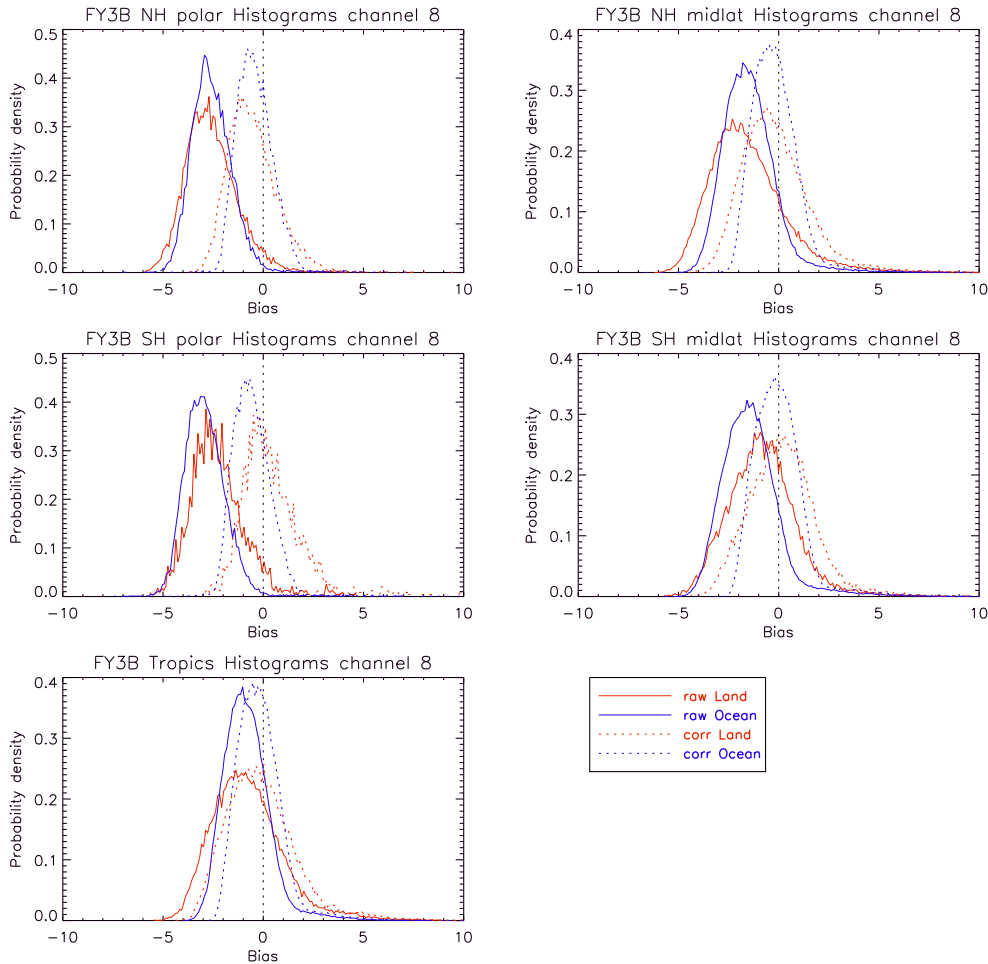


Figure 11: Same as Fig. 10 but for channel 8.

Analysis of scan dependency and scene temperature dependency based on April 22 to 26, 2015, were also conducted (not shown), and also resulted in very similar characteristics to those observed in the 2013 data.

Although based on a 5-day analysis, the similarity of MWHS-1 2015 with MWHS-1 2013 was estimated sufficient to be used in assimilation experiments.

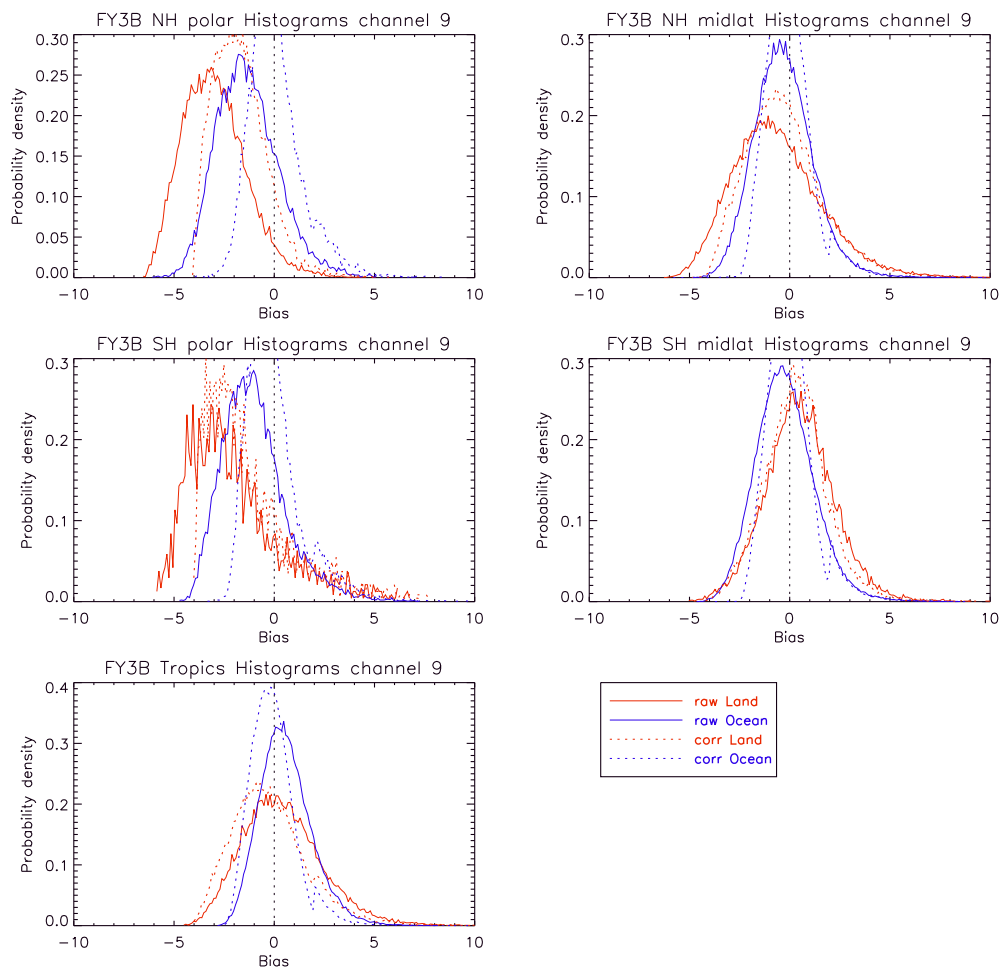


Figure 12: Same as Fig. 10 but for channel 9.

3 Assimilation Experiment

This section presents the results of the first assimilation experiment involving FY-3B humidity sounder, MWHS-1, in the MO global system. The experiment is also aimed at testing the impact of the VarBC correction scheme that will soon replace the current static bias correction. For this trial, MWHS-1 183 GHz channels are assimilated over ocean only, and the 150 GHz window channels are passively used for quality control purposes. FY-3B humidity sounder integrates here a body of five operationally-used microwave instruments of similar capability composed by ASMU-B/MHS and ATMS. In this context, the proper impact of MWHS-1 is not expected to be substantial, but most likely neutral to slightly positive, which would be consistent with the results from experiments conducted at ECMWF (Chen et al., 2014).

The trial period has been set to start on April 22, 2015, when FY-3B data have been re-archived. However, MWHS-1 observations were effectively assimilated only by April 24. The suite used for this trial is a copy of the control suite (mi-ae802), which uses the parallel suite 36 (v31.1.0) as baseline configuration, upgraded with FY-3B. The experiment was conducted until July 1, 2015, which represents 62 days not considering the spin up time (9 days). This section presents the analysis of the statistics produced in VAR, and the impact on the NWP index.

3.1 VAR statistics

Model forecasts are generated in 6-hour cycles, and each cycle serves as background field for the next one. VAR statistics help to compare model forecasts at a time T_n with the next cycle T_{n+6} . Statistics generated by the assimilation of independent observations remain unchanged between the control (without MWHS-1 data) and the experiment (with MWHS-1 data). Hence, any improvement or degradation in the fit to the model for the independent datasets can be seen as direct or indirect effect of the implementation of MWHS-1. It is necessary to make sure that no dataset are significantly degraded.

A key metric in the estimation of alterations induced by the assimilation of a new instrument is the change in standard deviation of the fit to the background for independent sounders. A significant reduction of standard deviation would be considered as an improvement from the new instrument, while an increase would be synonymous of degradation.

Figure 13 shows the relative standard deviation in O-B between the assimilation experiment and the control. The humidity sensitive channels of infrared instruments show little sensibility to the introduction of MWHS-1 (difference in standard deviation less than $\pm 1\%$). Although the impact is also neutral in AIRS and IASI temperature sensitive channels, CRIS temperature sensitive channels respond to the addition of the new instrument with more variability ($\pm 2.5\%$). A significant reduction of the standard deviation, consistent for all hyperspectral infrared instruments, is observed in the window sensitive channels. However, it must be noted that this reduction in standard deviation is accompanied by an increase of the observation counts, by 21, 6, and 1% for AIRS, CRIS, and IASI,

respectively, and therefore do not necessarily signify an improved fit to the model. Note that there is a known issue with the bias correction of window channels for advanced IR sounders in VarBC. This problem is currently under investigation, but the positive impact of MWHS-1, although unexpected, is encouraging.

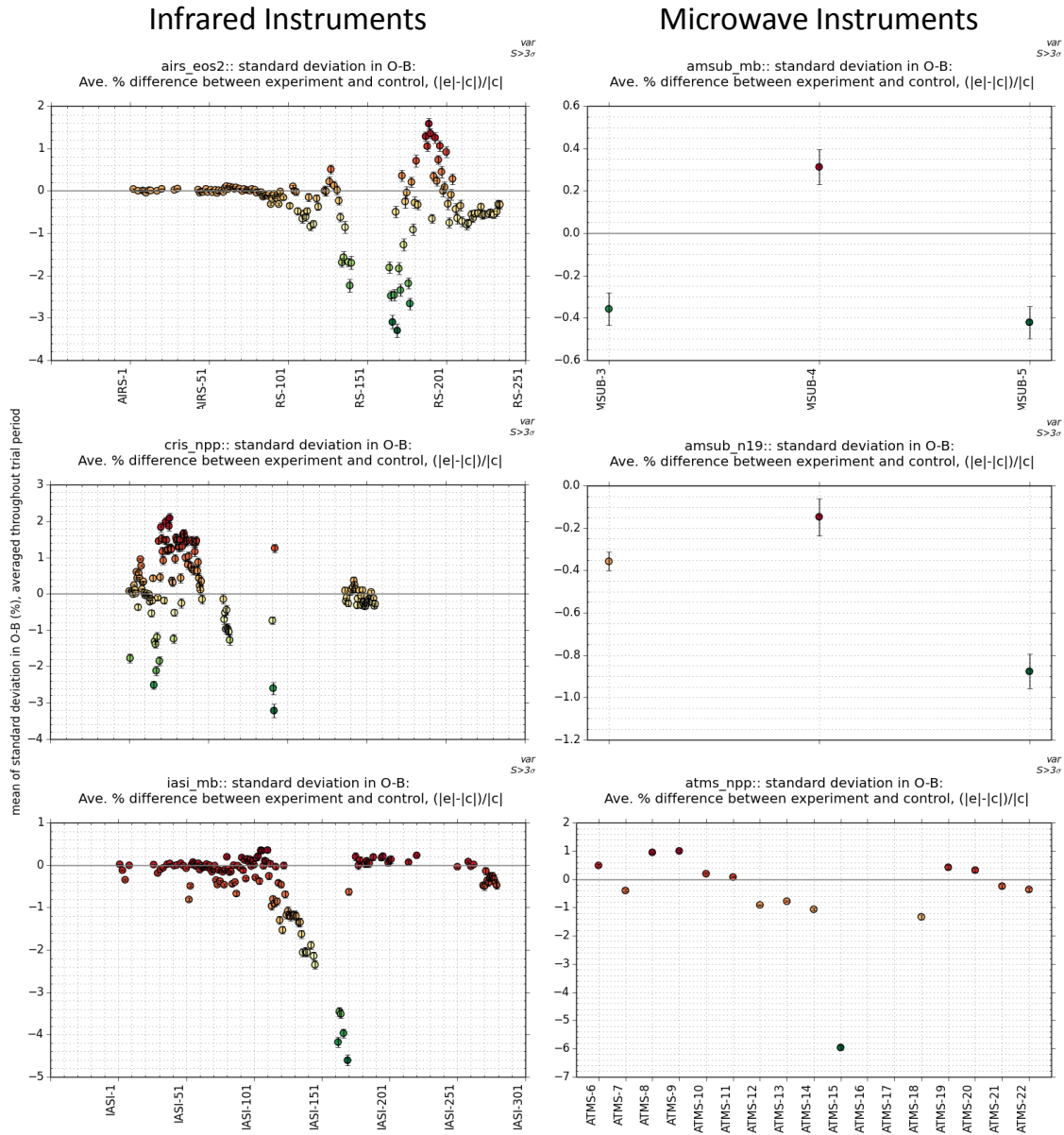


Figure 13: Relative standard deviation (%) in O-B between the assimilation experiment and the control. (Left from top to bottom) Infrared instruments: AIRS, CRIS, and IASI (MetOp-B). (Right from top to bottom) Microwave instruments: AMSU-B (MetOp-B and NOAA19) and ATMS.

Similarly, the impact on the standard deviation in O-B for microwave instruments remains mostly neutral with a variability comprised within $\pm 0.4\%$ for AMSU-B on MetOp-B and $\pm 1.2\%$ for ATMS (except channel 15). Only AMSU-B on NOAA19 shows a consistent 0.1-0.9% reduction in standard deviation throughout all its channels. No significant change in observation counts is observed for

microwave instruments.

Finally, VAR statistics also informs on the average magnitude of the mean departure of MWHS-1 in the VarBC scheme. Departure for MWHS-1 channels 3, 4 and 5 are 0.010 ± 0.008 , 0.016 ± 0.002 , and 0.011 ± 0.004 , respectively. The VarBC scheme represents a significant improvement since the departure are roughly reduced by 1 to 2 orders of magnitude compared to the static correction scheme.

3.2 NWP index

When computing a NWP index, the total impact of the assimilation of a new instrument is estimated by comparison against both sonde observations and analysis. The index is obtained from a weighted average of forecast fields (temperature, height, relative humidity, wind speed, and pressure at different levels). Weights are determined to better reflect MO customers needs. Two versions of the index are currently used: a pre-2012 version, referred to as *old* version, where shorter range forecasts receive the highest weights, and a post-2012 version, referred to as *new* version, where higher weighting is assigned to longer range forecasts. Weston (2014) showed that this difference impacts the significance of the result. For short experiments (less than 6 weeks), the old index appears to be the most relevant analysis as it offers a smaller significance window ($\pm 0.25\%$ compared to $\pm 0.4\%$ for the new index, after 30 days of experiment).

Figure 14 (left) shows the experiment-control difference in forecast root mean square (RMS) error for an extended selection of parameters of the old index compared to observations. Negative RMS difference is synonymous of improvement while positive RMS difference is synonymous of degradation. In the Northern hemisphere (top), the RMS difference is mostly positive but broadly insignificant. The shortness of the assimilation period makes the analysis of the longest forecast time inconclusive. In the Tropics (middle), both positive and negative RMS difference are observed. The noteworthy features are the deterioration of short-range forecasts for H500 and stratospheric temperature T50. In contrast, height H50 forecasts improve with RMS difference down to -7%. In the Southern hemisphere (bottom), most improvements with a significant level affect long-range forecasts and are thus inconclusive. Short-range forecasts of H700, H500, H250, H100, and tropospheric temperature T700 result to have deteriorated at significant levels.

Figure 14 (right) shows the parameters compared to analyses. The main differences with respect to the comparison with observations are observed in the Tropics and in the Southern hemisphere. In the Tropics, particularly noteworthy is the RMS difference significantly negative for H500. In the Southern hemisphere, all significantly negative RMS difference are short-range forecast (W100, H100, T250, and T500). However, a large degradation of RH500 is observed at short-range with RMS difference greater than 7%. H850, H700, T850, T700, and RH700 also significantly degrade.

The resulting index is neutral to slightly negative both in the old version (-0.373 vs observations and -0.369 vs analyses) and in the new version (-0.207 vs observations).

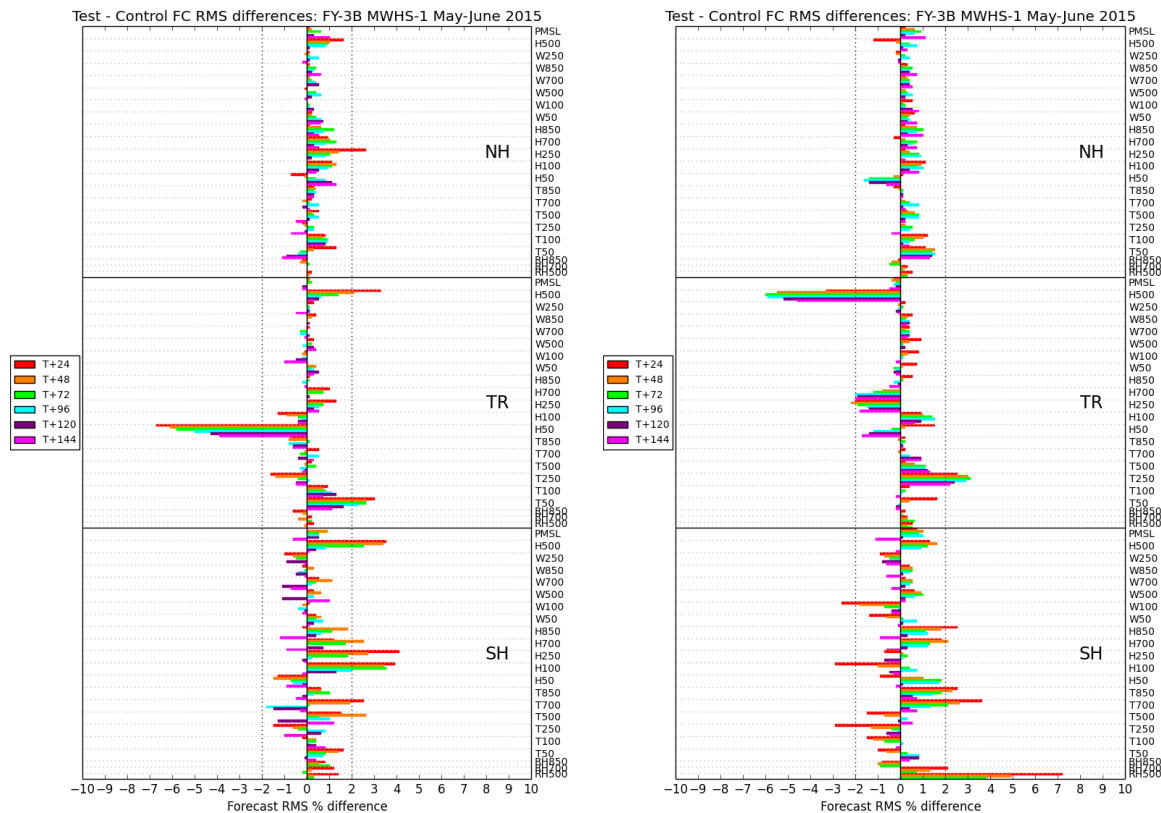


Figure 14: (Left) Experiment minus control difference in forecast RMS error compared to observations, with forecast time-range from 24 to 144 h, in the Northern hemisphere, Tropics, and Southern hemisphere. (Right) Same as left but compared to analyses.

Concluding remarks

This document presents the assessment of one year of observation from MWTS-1 and MWHS-1 on board the Chinese FY-3B platform. Preliminary results from the assimilation of MWHS-1 183 GHz channels in the Met Office NWP model are also introduced.

MWTS-1 window channels 1 (50.3 GHz), and tropospheric channels 2 (53.6 GHz) and 3 (54.94 GHz) have been analyzed. The mean first guess departure from raw observations (O-B) was found to vary by nearly two orders of magnitude between Ch. 1, characterized by the largest bias (1.42 K over ocean), and Ch. 2, which biases range from -0.12 to -0.27 K depending on the surface type. Although surface type has little influence on Ch. 3 biases, the month-to-month variability is however more irregular than in the two other channels. A scan position dependency was observed for all channels, independently of the season or the surface type. MWTS-1 is also affected by a radiometer non-linearity resulting in a first guess departure dependent on the scene temperature, thoroughly studied in previous assessment works (references therein), and therefore not further detailed in this report. The bias analysis presented in this document shows that the Met Office static correction scheme efficiently handles the highlighted biases, reducing the first guess departure to values ranging from -0.1 to -0.24 K, all MWHTS-1 channels considered. The correction scheme also reduce the seasonal variability and the scan position dependency.

For MWHS-1, the window channels 5 and 6 (150 GHz), and the tropospheric channels 7, 8, and 9 (183 GHz) have been studied. Window channels O-B greatly vary with the surface type (<0.9 K over land, >6K over ocean, and >12 K over ice) as well as with the season. On the contrary, tropospheric channels variations with surface types are small (O-B ranging from -0.86 to -2.25 K) and almost not affected by seasonal cycles. One exception is a surprising ~1K difference between O-B over land and O-B over ocean in the Southern hemisphere mid-latitudes. With a peak of sensitivity in the upper, mid, and lower-troposphere, Chs. 7, 8, and 9, respectively, should not be affected by surface types. However, because this feature is only observed in the southern mid-latitudes, this suggests that it can result, at least partly, from a sampling effect. Like the temperature sounder, MWHS-1 displays scan position dependent biases. A radiometer non-linearity was also identified in Chs. 7, 8, and 9, with O-B mostly negative in the temperature lower range and mostly positive in the temperature upper range. Nonetheless, the static correction scheme proved again to efficiently reduce the biases (183 GHz departures after correction smaller than -1.03 K), the seasonal variability, and both scan position and scene temperature dependency. It is however not true for MWHS-1 window channels departures, which remain either unchanged or are degraded after correction. The large biases observed in the 150 GHz channels do not preclude the assimilation of MWHS-1 in the Met Office NWP model as those channels are used passively for quality control purpose only.

The analysis of a 62-day assimilation experiment with MWHS-1 183 GHz channels showed an overall neutral impact on the NWP indexes. The further examination of different key parameters revealed however a more mixed picture with significant degradation of the tropospheric relative

humidity in the Southern hemisphere. Var statistics showed a reduced standard deviation of the fit to the background for window sensitive channels of infrared sounders, but with an increase of the observation counts that prevents to conclude whether the fit to the background is really improved or not.

Future work

MWTS-1 failed in 2014 and the following platform (FY-3C) carries the MWTS-2 instrument, an advanced version of MWTS-1, therefore no further analysis of the FY-3B temperature sounder is planned to date.

Since MWHS-1 is still operational, and aimed to be operationally assimilated in the MO NWP model, additional evaluations should be carried forward in order to guarantee the best data quality. This includes : 1) the study of the impact of an error rescaling by $N\Delta T$ ratio of similar instrument, 2) the better comprehension of the 1 K difference between land and ocean O-B in the southern mid-latitudes, and 3) the investigation of the origin of the relative humidity RMS forecast error degradation in the Southern hemisphere.

Acknowledgments

We gratefully acknowledge the support of the Climate Science for Service Partnership: China (CSSP) program at the MetOffice for supporting the work of Katie Lean and Nigel Atkinson and the National Satellite Meteorological Center (NSMC) of Chinese Meteorological Administration (CMA) for their contribution to this work. The European Union's Horizon-2020 programme GAIA-CLIM project has supported the work of Fabien Carminati and William Bell.

Appendix A

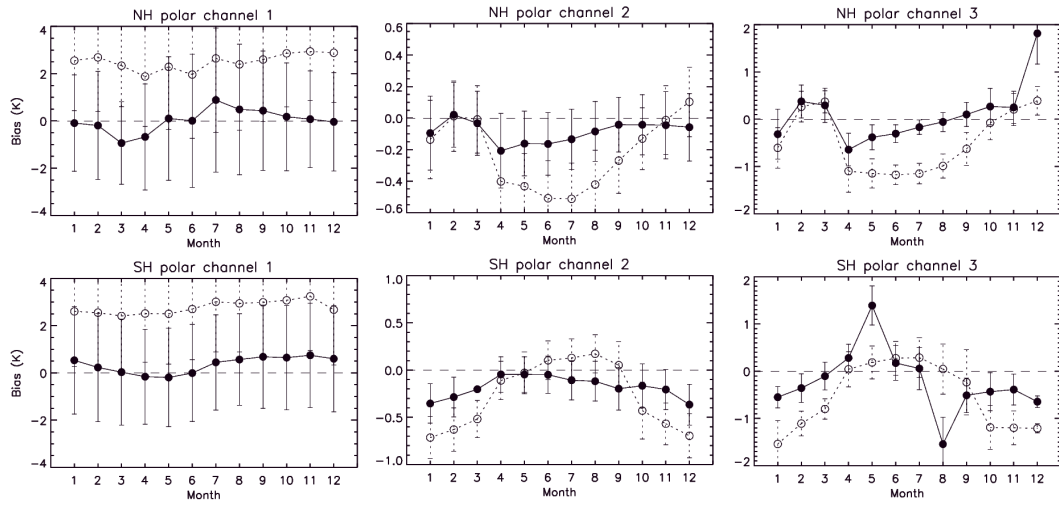


Figure A.1: (Top, from left to right) Monthly averaged O-B (circles), C-B (filled circles), and 1σ standard deviation (dashed and solid vertical bars, respectively) for MWTS-1 channels 1 to 3 over polar latitudes oceanic surface in the northern hemisphere. (Bottom) Same as top, but for the southern hemisphere.

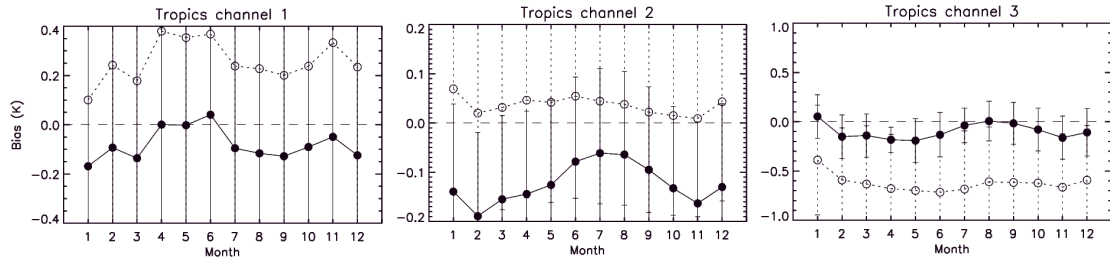


Figure A.2: Same as Fig. A.1 but for tropical latitudes.

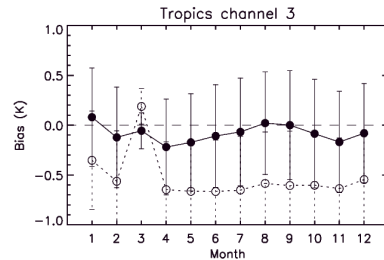


Figure A.3: Same as Fig. A.1 but for tropical land surface, channel 3 only.

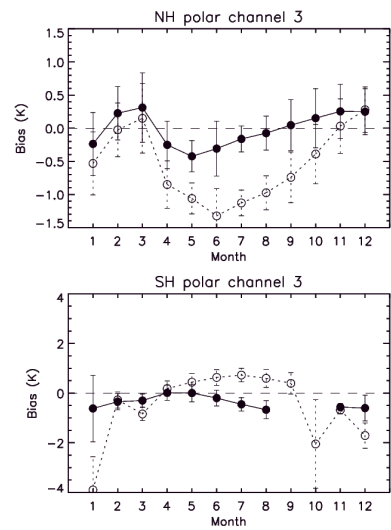


Figure A.4: Same as Fig. A.1 but for land surface, channel 3 only.

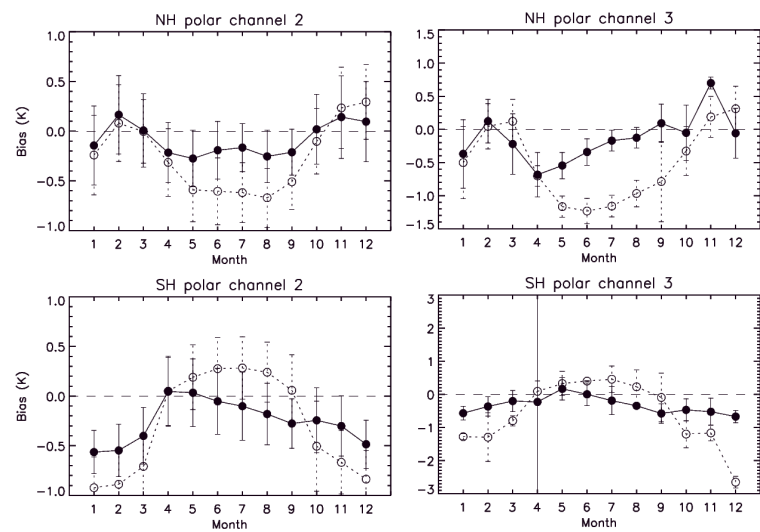


Figure A.5: Same as Fig. A.1 but for sea ice surface, channels 2 and 3 only.

Appendix B

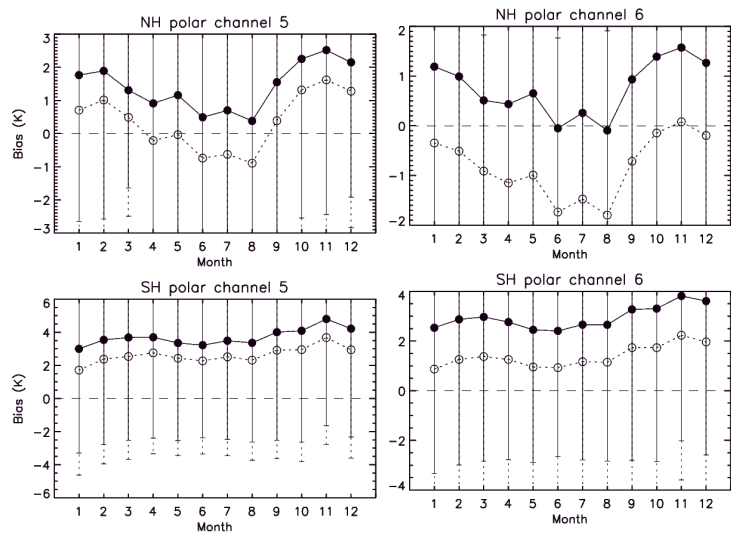


Figure B.1: (Top, from left to right) Monthly averaged O-B (circles), C-B (filled circles), and 1σ standard deviation (dashed and solid vertical bars, respectively) for MWHS-1 channels 5 and 6 over polar latitudes oceanic surface in the northern hemisphere. (Bottom) Same as top, but for the southern hemisphere.

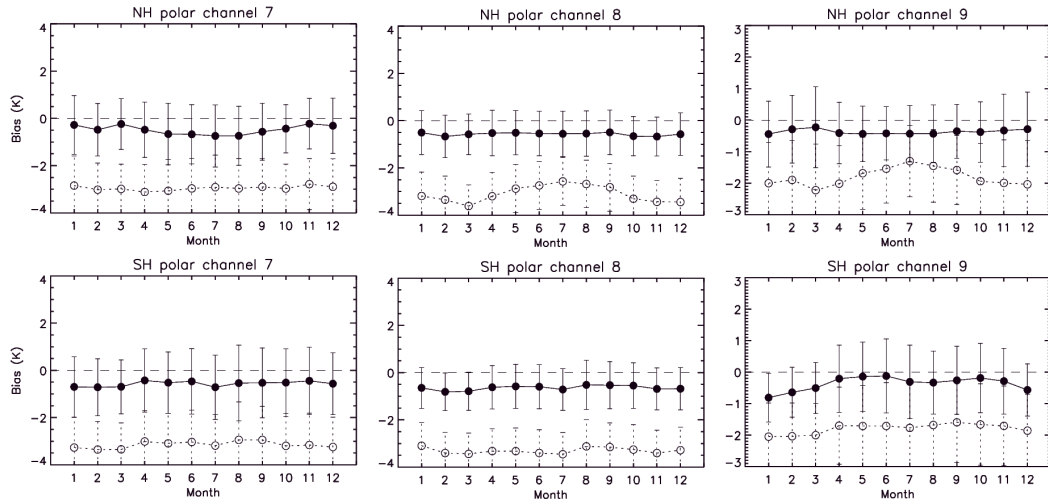


Figure B.2: Same as Fig. B.1 but for channels 7, 8, and 9.

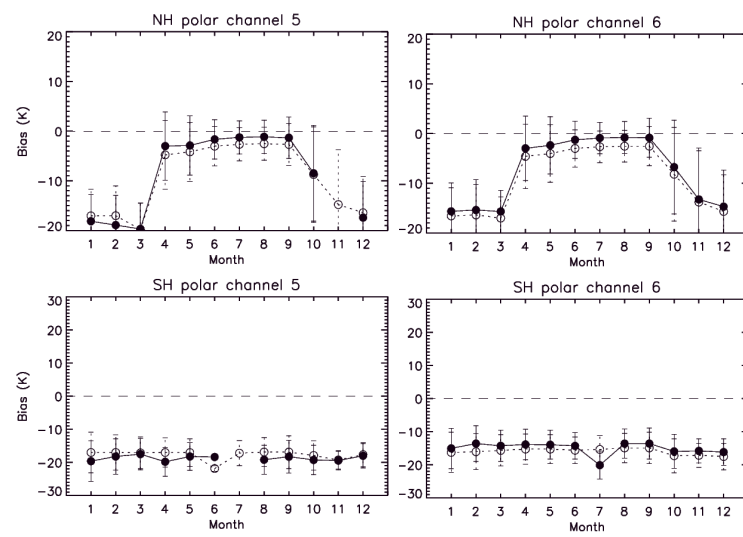


Figure B.3: Same as Fig. B.1 but for land surface.

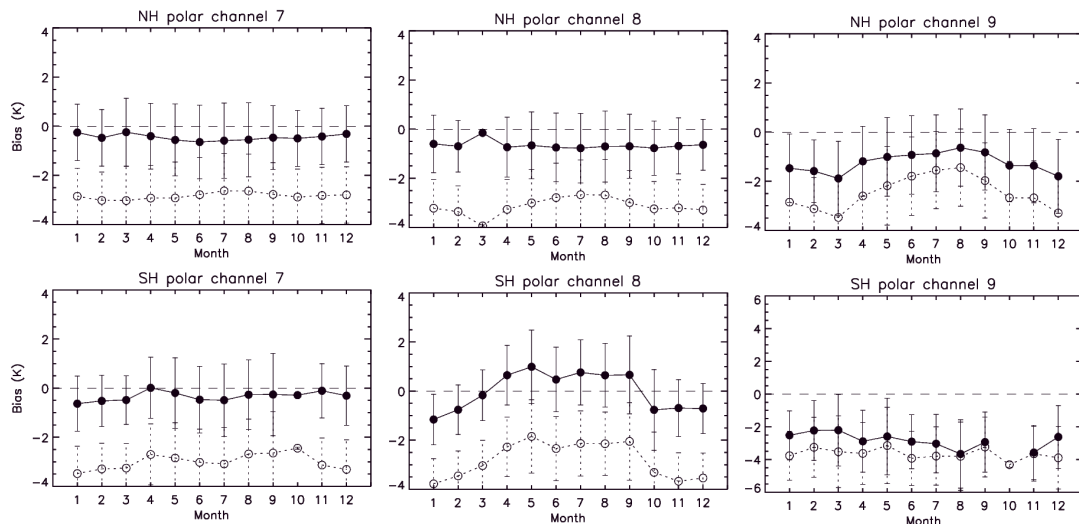


Figure B.4: Same as Fig. B.1 but for land surface channels 7, 8, and 9.

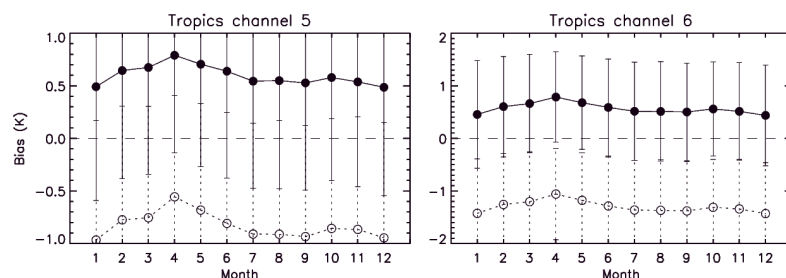


Figure B.5: Same as Fig. B.1 but for tropical latitudes.

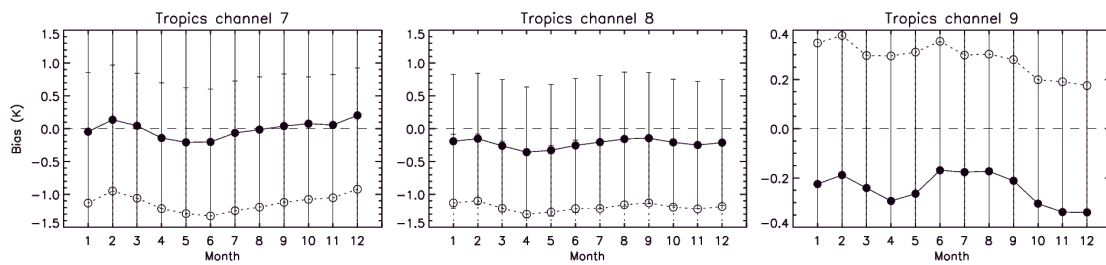


Figure B.6: Same as Fig. B.1 but for tropical latitudes channels 7, 8, and 9.

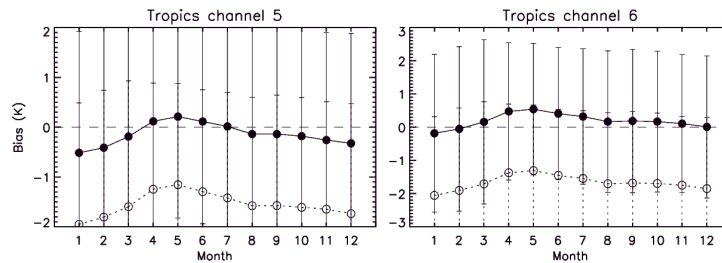


Figure B.7: Same as Fig. B.1 but for tropical latitudes land surface.

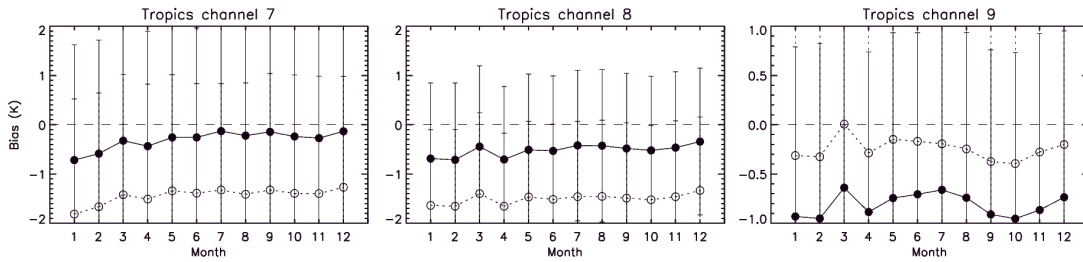


Figure B.8: Same as Fig. B.1 but for tropical latitudes land surface channels 7, 8, and 9.

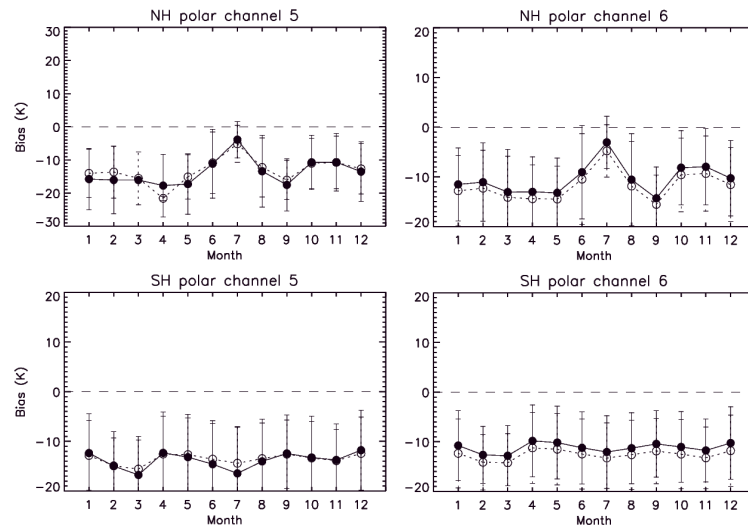


Figure B.9: Same as Fig. B.1 but for sea ice surface.

Appendix C

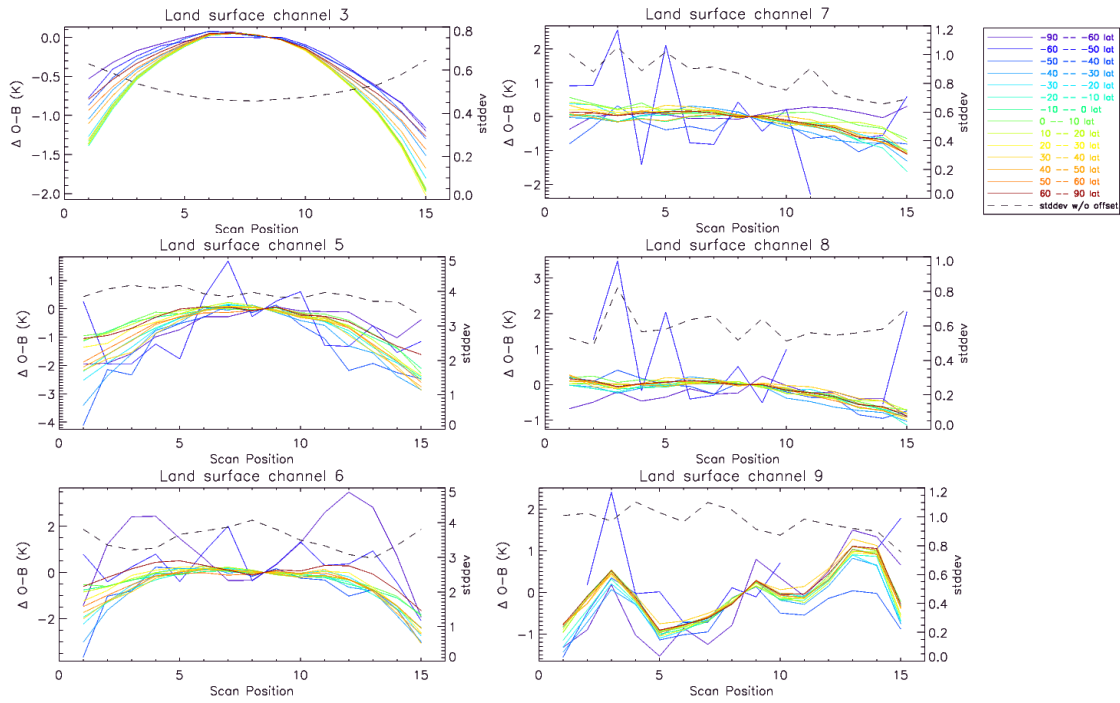


Figure C.1: (From top to bottom and left to right) MWTS-1 channel 3 and MWHS-1 channels 5 to 9 variations in first guess departure in raw observations ($\Delta O - B$) as a function of scan position in 14 latitude bands over land surface in July 2013. An offset was applied so that all $\Delta O - B$ are set to zero on the middle of the scan. Black dashed line shows the 1σ standard deviation of $\Delta O - B$ before offset.

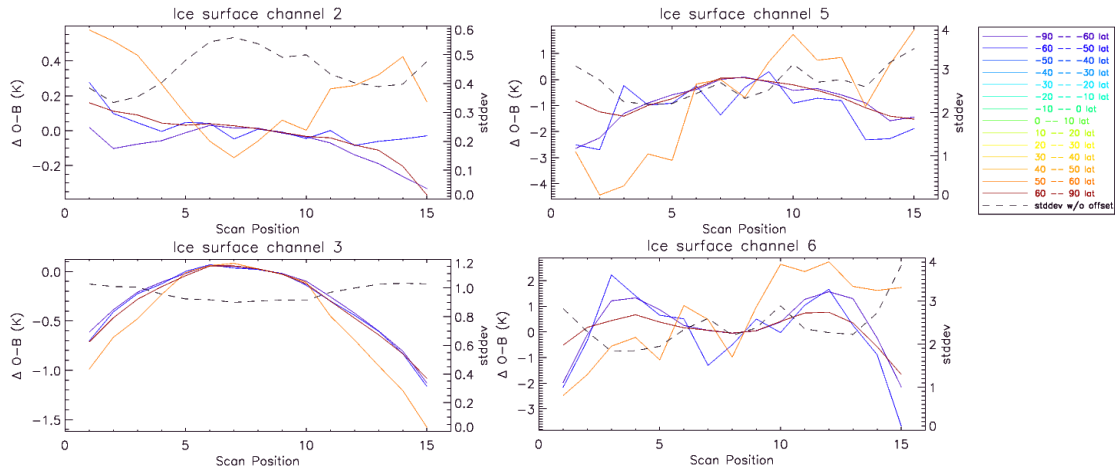


Figure C.2: Same as Fig. C.1 but for MWTS-1 channels 2 and 3, and MWHS-1 channels 5 and 6 over sea ice surface.

Appendix D

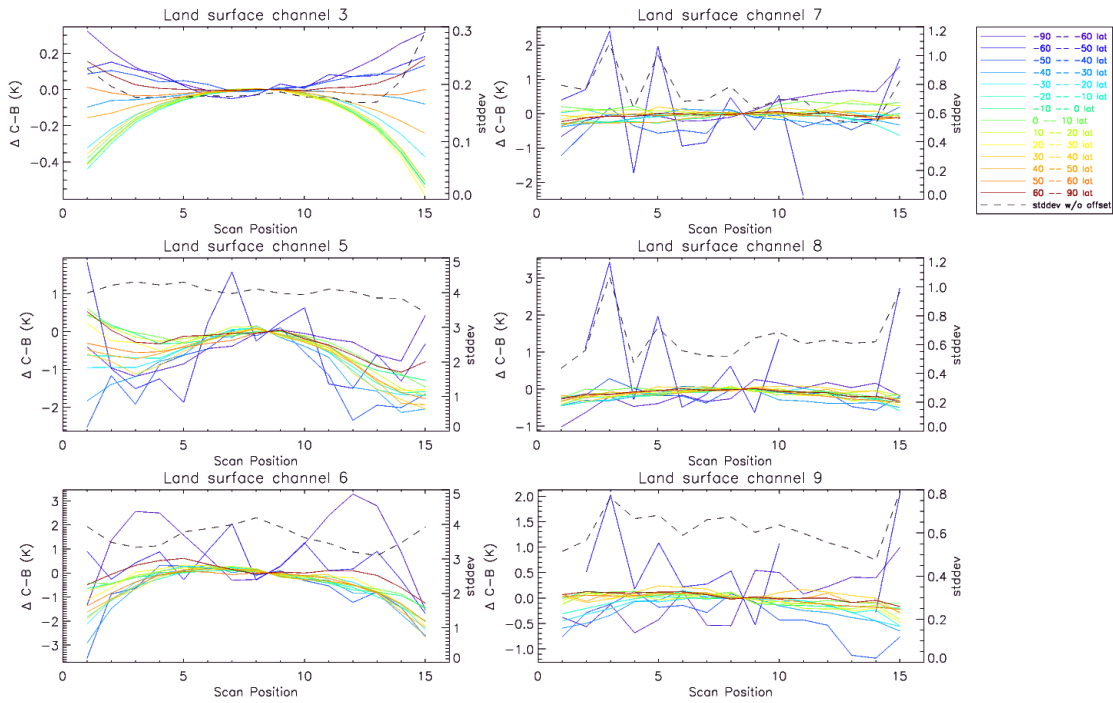


Figure D.1: (From top to bottom and left to right) MWTS-1 channel 3 and MWHS-1 channels 5 to 9 variations in first guess departure in corrected observations ($\Delta C-B$) as a function of scan position in 14 latitude bands over land surface in July 2013. An offset was applied so that all $\Delta C-B$ are set to zero on the middle of the scan. Black dashed line shows the 1σ standard deviation of $\Delta C-B$ before offset.

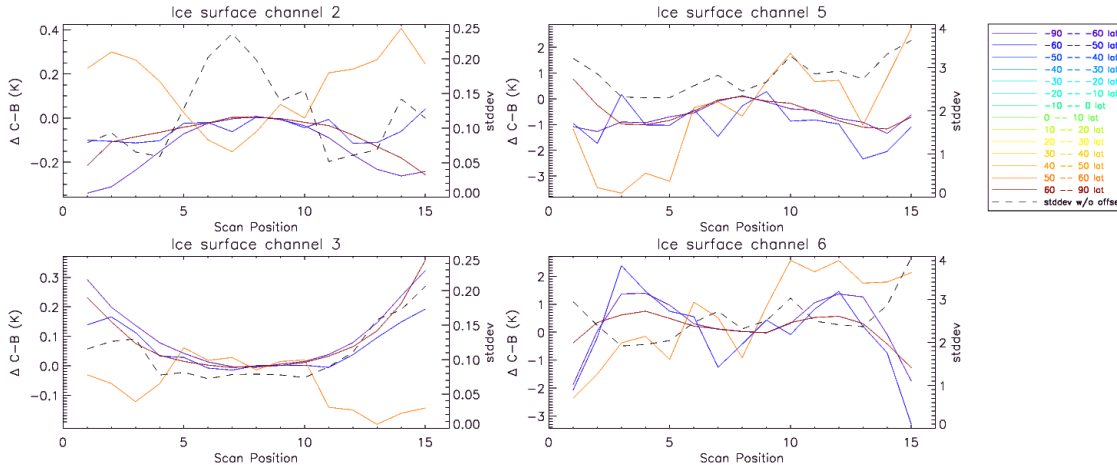


Figure D.2: Same as Fig. D.1 but for MWTS-1 channels 2 and 3, and MWHS-1 channels 5 and 6 over sea ice surface.

Appendix E

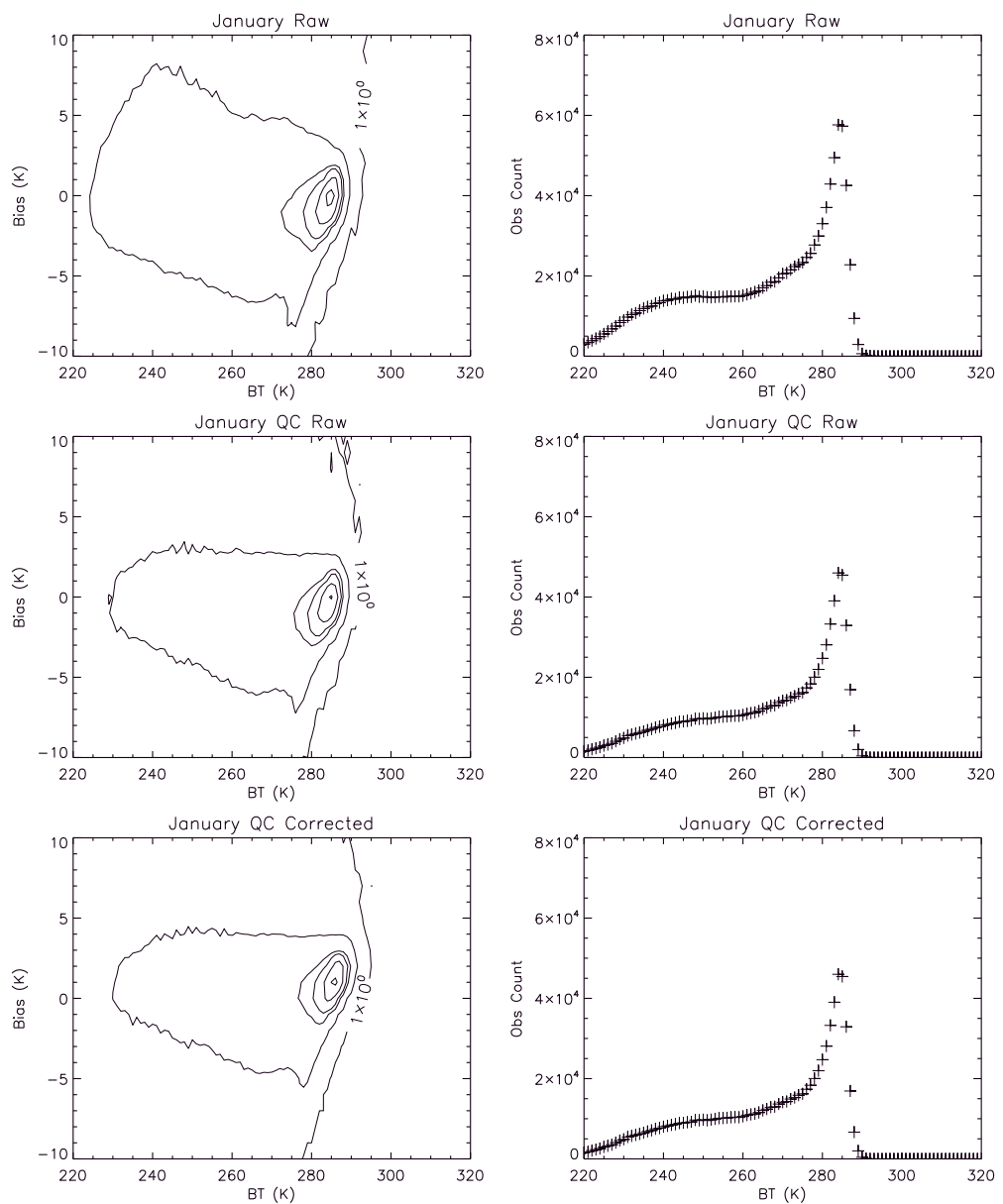


Figure E.1: (Left) Distribution of MWHS-1 channel 5 O-B before quality control (top), quality control screened O-B (middle), and screened C-B (bottom) as a function of the brightness temperature (BT) in January 2013. (Right) Number of raw (top), screened raw (middle), and screened corrected observations (bottom).

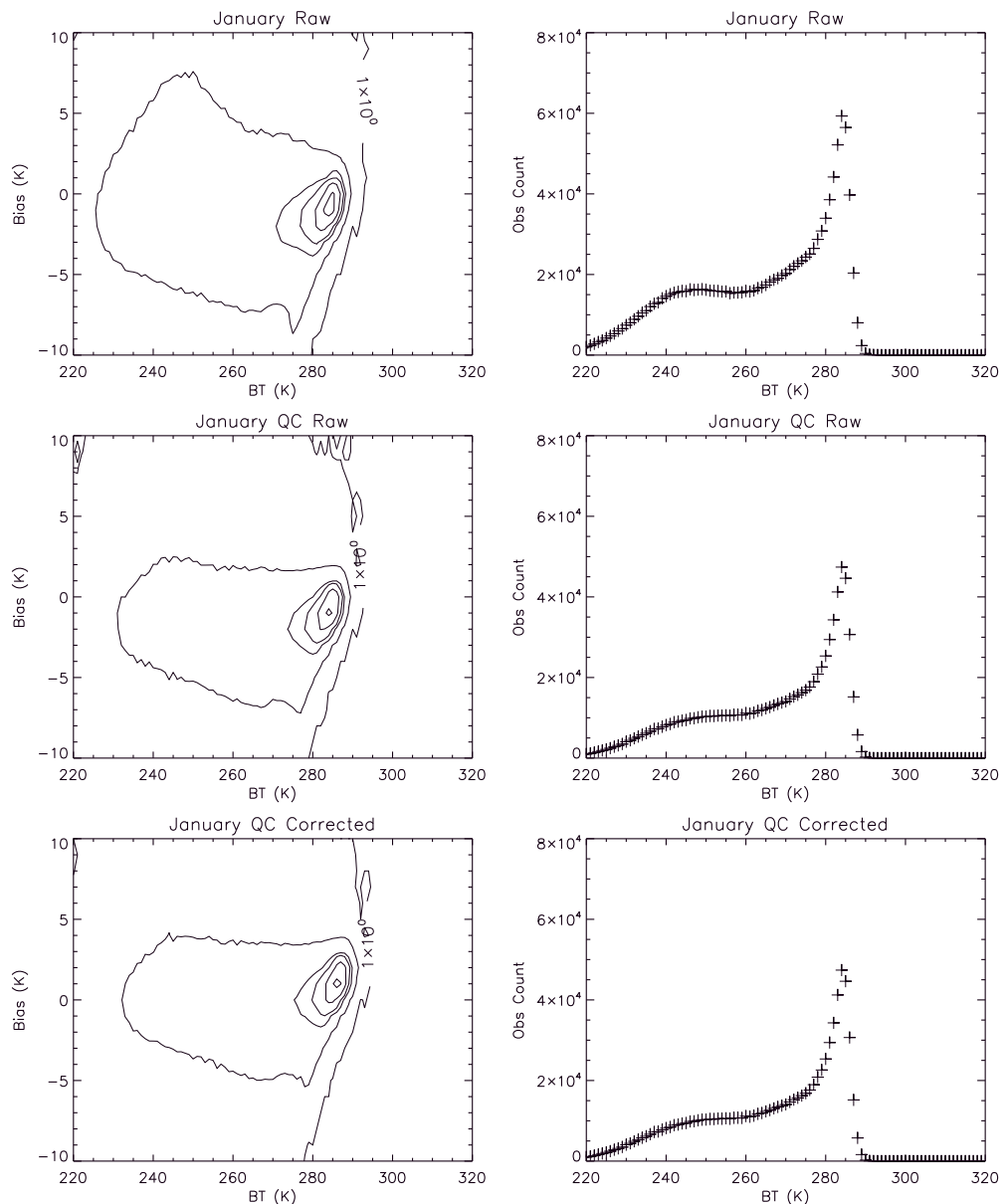


Figure E.2: Same as Fig. E.1 but for channel 6.

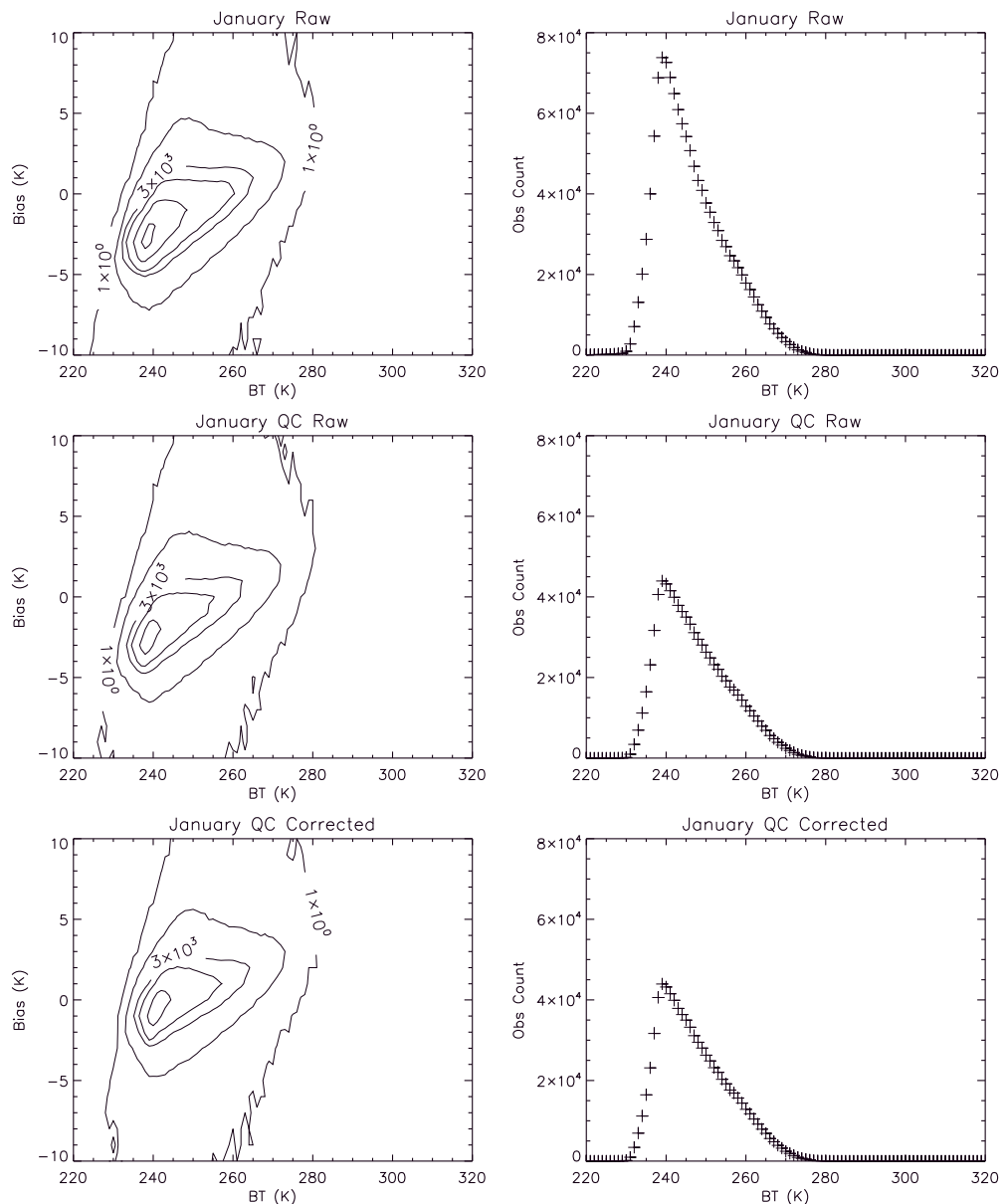


Figure E.3: Same as Fig. E.1 but for channel 7.

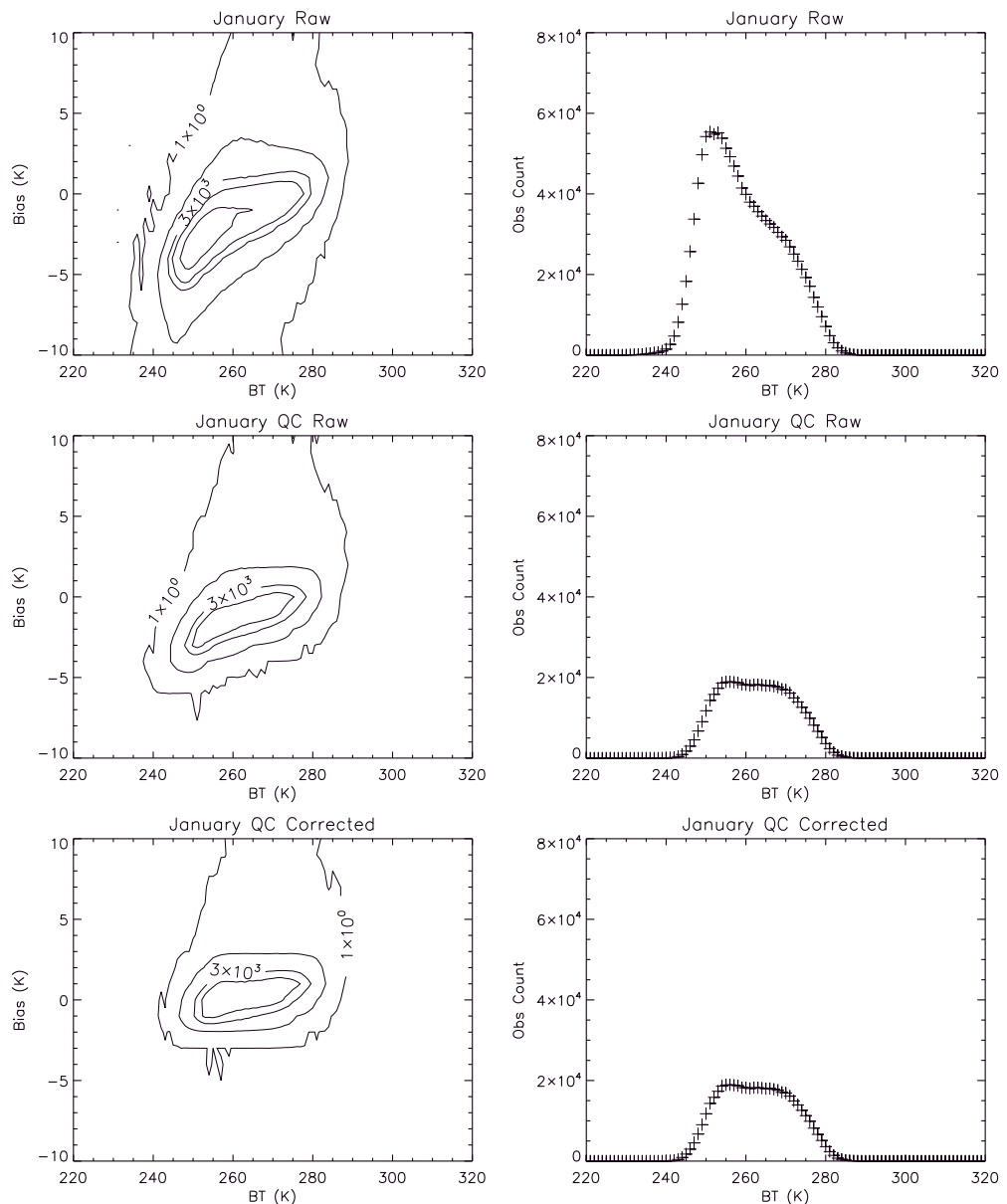


Figure E.4: Same as Fig. E.1 but for channel 8.

References

- [1] James Cameron. Options for the development of varbcat the met office and recommendations-for operational implementation at ps37. *Met Office Satellite Applications Technical Memos*, (25), 2015.
- [2] Keyi Chen, Stephen English, and Jiang Zhu. Assessment of fy3a and fy3b/mwhs observations. *ECMWF Technical Memorandum*, (734), 2014.
- [3] A Doherty, N Atkinson, W Bell, B Candy, S Keogh, and C Cooper. An initial assessment of data from the advanced technology microwave sounder. *Forecast R&T Reopot*, (569), 2012.
- [4] Chaohua Dong, Jun Yang, Zhongdong Yang, Naimeng Lu, Jinming Shi, Peng Zhang, Yujie Liu, Bin Cai, and Wenjian Zhang. An overview of a new chinese weather satellite fy-3a. *Bulletin of the American Meteorological Society*, 90(10):1531–1544, 2009.
- [5] BA Harris and G Kelly. A satellite radiance-bias correction scheme for data assimilation. *Quarterly Journal of the Royal Meteorological Society*, 127(574):1453–1468, 2001.
- [6] Qifeng Lu, W Bell, P Bauer, N Bormann, and C Peubey. An evaluation of fy-3a satellite data for numerical weather prediction. *Quarterly Journal of the Royal Meteorological Society*, 137(658):1298–1311, 2011.
- [7] Qifeng Lu, William Bell, Peter Bauer, Niels Bormann, and Carole Peubey. Characterizing the fy-3a microwave temperature sounder using the ecmwf model. *Journal of Atmospheric and Oceanic Technology*, 28(11):1373–1389, 2011.
- [8] Qifeng Lu, William Bell, N Bormann, P Bauer, C Peubey, and AJ Geer. Improved assimilation of data from china's fy-3a microwave temperature sounder. *Atmospheric Science Letters*, 13(1):9–15, 2012.
- [9] Peter Weston. The statistical significance of assimilation trial results: Case study on sa package trials for ps34. *Met Office Satellite Applications Technical Memos*, (22), 2014.
- [10] X Zou, X Wang, F Weng, and G Li. Assessments of chinese fengyun microwave temperature sounder (mwts) measurements for weather and climate applications. *Journal of Atmospheric and Oceanic Technology*, 28(10):1206–1227, 2011.

Met Office Tel: 0370 900 0100
FitzRoy Road, Exeter Fax: 0370 900 5050
Devon, EX1 3PB enquiries@metoffice.gov.uk
UK www.metoffice.gov.uk